STABILITY-DERIVATIVE DETERMINATION FROM FLIGHT DATA

By Chester H. Wolowicz and Euclid C. Holleman

High-Speed Flight Station
Edwards, Calif., U.S.A.

Presented to Flight Test Panel
of the Advisory Group for
Aeronautical Research and Development

Copenhagen, Denmark
October 20-25, 1958

NATIONAL AERONAUTICS AND SPACE ADMINISTRATION
WASHINGTON

N-65068X

STABILITY-DERIVATIVE DETERMINATION FROM FLIGHT DATA

By Chester H. Wolowicz and Euclid C. Holleman

SUMMARY

A comprehensive discussion of the various factors affecting the determination of stability and control derivatives from flight data is presented based on the experience of the NASA High-Speed Flight Station. Factors relating to test techniques, determination of mass characteristics, instrumentation, and methods of analysis are discussed.

For most longitudinal-stability-derivative analyses simple equations utilizing period and damping have been found to be as satisfactory as more comprehensive methods. The graphical time-vector method has been the basis of lateral-derivative analysis, although simple approximate methods can be useful if applied with caution. Control effectiveness has been generally obtained by relating the peak acceleration to the rapid control input, and consideration must be given to aerodynamic contributions if reasonable accuracy is to be realized.

Because of the many factors involved in the determination of stability derivatives, it is believed that the primary stability and control derivatives are probably accurate to within 10 to 25 percent, depending upon the specific derivative. Static-stability derivatives at low angle of attack show the greatest accuracy.

INTRODUCTION

The flight-determined aerodynamic stability and control derivatives are of much value to the flight-test analyst inasmuch as these derivatives may be compared to wind-tunnel measurements for substantiation of the predicted behavior of the airplane. Thus the determination of stability derivatives has become an important part of flight testing and has, in some instances, revealed characteristics that the wind tunnel was unable to predict. Where wind-tunnel data are unavailable or where the safety of flight into untested regions is of concern, flight-determined derivatives have been used to predict airplane behavior prior to flight into these regions.

Because of the exploratory nature of many of the investigations conducted at the NASA High-Speed Flight Station, the practical aspects of determining derivatives from flight data have been of extreme importance. It is the primary purpose of this paper to discuss a number of factors that influence the determination of stability and control derivatives from flight data. Among the factors discussed are test techniques, mass characteristics, instrumentation, and methods of extracting both primary and secondary derivatives.

SYMBOLS AND COEFFICIENTS

Flight data shown in the figures are referenced to the body system of axes (fig. 1), as are the equations of motion (appendix A).

a	perpendicular distance from spring to knife edge
a_x, a_t, a_n	longitudinal, transverse, and normal accelerations of aircraft at the center of gravity, g units
$a_{x_l}, a_{t_l}, a_{n_l}$	recorded values of a_x, a_t, and a_n corrected for instrument phase lag and misalinement but not for location relative to the center of gravity, g units
b	wing span, ft
C_A	axial-force coefficient
$C_{D'}$	drag coefficient, $\frac{\text{Drag (approx.)}}{\bar{q}S}$
C_L	lift coefficient, $\frac{\text{Lift}}{\bar{q}S}$
C_{L_t}	trim 1 g lift coefficient, $\frac{W}{\bar{q}S}$
C_{L_α}	lift-curve slope, $\frac{\partial C_L}{\partial \alpha}$
C_l	rolling-moment coefficient, $\frac{\text{Rolling moment}}{\bar{q}Sb}$
C_{l_p}	damping-in-roll derivative, $\frac{\partial C_l}{\partial \frac{pb}{2V}}$, per radian
C_{l_r}	rate of change of rolling-moment coefficient with yawing angular-velocity factor, $\frac{\partial C_l}{\partial \frac{rb}{2V}}$, per radian
C_{l_β}	effective dihedral derivative, $\frac{\partial C_l}{\partial \beta}$, per radian
$C_{l_{\dot{\beta}}}$	rate of change of rolling-moment coefficient with rate of change of angle-of-sideslip factor, $\frac{\partial C_l}{\partial \frac{\dot{\beta}b}{2V}}$, per radian

C_{l_δ} rate of change of rolling-moment coefficient with respect to pertinent control-surface displacement, $\frac{\partial C_l}{\partial \delta}$, per radian

C_m pitching-moment coefficient, $\frac{\text{Pitching moment}}{\bar{q}S\bar{c}}$

C_{m_α} longitudinal stability derivative, $\frac{\partial C_m}{\partial \alpha}$, per radian

$C_{m_{\dot{\alpha}}}$ $\frac{\partial C_m}{\partial \frac{\dot{\alpha}\bar{c}}{2V}}$, per radian

C_{m_β} $\frac{\partial C_m}{\partial \beta}$, per radian

C_{m_δ} $\frac{\partial C_m}{\partial \delta}$, per radian

C_{m_q} $\frac{\partial C_m}{\partial \frac{q\bar{c}}{2V}}$, per radian

C_N normal-force coefficient, $\frac{\text{Normal force}}{\bar{q}S}$

C_{N_α} $\frac{\partial C_N}{\partial \alpha}$, per radian

$C_{N_{\dot{\alpha}}}$ $\frac{\partial C_N}{\partial \frac{\dot{\alpha}\bar{c}}{2V}}$, per radian

C_{N_q} $\frac{\partial C_N}{\partial \frac{q\bar{c}}{2V}}$, per radian

C_{N_δ} $\frac{\partial C_N}{\partial \delta}$, per radian

C_n yawing-moment coefficient, $\frac{\text{Yawing moment}}{\bar{q}Sb}$

C_{n_p} rate of change of yawing-moment coefficient with rolling angular-velocity factor, $\frac{\partial C_n}{\partial \frac{pb}{2V}}$, per radian

C_{n_r} rate of change of yawing-moment coefficient with yawing angular-velocity factor, $\frac{\partial C_n}{\partial \frac{rb}{2V}}$, per radian

C_{n_β} directional stability derivative, $\frac{\partial C_n}{\partial \beta}$, per radian

$C_{n_{\dot{\beta}}}$ rate of change of yawing-moment coefficient with rate of change of angle-of-sideslip factor, $\frac{\partial C_n}{\partial \frac{\dot{\beta}b}{2V}}$, per radian

C_{n_δ} rate of change of yawing-moment coefficient with respect to pertinent control-surface displacement, $\frac{\partial C_n}{\partial \delta}$, per radian

C_Y transverse-force coefficient, $\frac{\text{Transverse force}}{\bar{q}S}$

C_{Y_p} $\frac{\partial C_Y}{\partial \frac{pb}{2V}}$, per radian

C_{Y_r} $\frac{\partial C_Y}{\partial \frac{rb}{2V}}$, per radian

C_{Y_β} lateral-force derivative, $\frac{\partial C_Y}{\partial \beta}$, per radian

$C_{Y_{\dot{\beta}}}$ $\frac{\partial C_Y}{\partial \frac{\dot{\beta}b}{2V}}$, per radian

C_{Y_δ} $\frac{\partial C_Y}{\partial \delta}$, per radian

$\bar{c}$ mean aerodynamic chord, ft

g acceleration of gravity, ft/sec^2

h_p pressure altitude, ft

I_X, I_Y, I_Z moments of inertia referred to body axes, slug-ft^2

I_{XZ} product of inertia referred to body X- and Z-axes, slug-ft^2

$I_{X_O}, I_{Y_O}, I_{Z_O}$	moments of inertia referred to principal system of axes, slug-ft^2
I_{X_e}	moment of inertia of rotating mass of the engine relative to its axis of rotation, slug-ft^2
K	linear spring constant, lb/ft
K_t	torsional spring constant, ft-lb/radians
L	rolling moment, ft-lb
M	Mach number
m	mass of airplane, W/g, slugs
N	yawing moment, ft-lb
P	period of oscillation, sec
p,q,r	rolling, pitching, and yawing angular velocity, respectively, radians/sec
$\dot{p},\dot{q},\dot{r}$	rolling, pitching, and yawing acceleration, respectively, radians/sec^2
p'	helix angle, pb/2V, radians
$\bar{p}$	average rolling velocity, radians/sec
$\bar{q}$	dynamic pressure, $1/2\rho V^2$, lb/sq ft
r'	yawing angular velocity factor, rb/2V, radians
S	wing area, sq ft
T	engine thrust, lb
$T_{1/2}$	time required for absolute value of transient oscillation to damp to half amplitude, sec
t	time, sec
V	airspeed, ft/sec
u,v,w	linear velocities relative to X-, Y-, and Z-axes, respectively, ft/sec
$\dot{v},\dot{w}$	transverse and normal linear accelerations, respectively, ft/sec^2

W	weight of aircraft, lb
W_c	weight of cradle, lb
x,y,z	distances, ft
z_e	normal distance from center of gravity to thrust line of engine, ft
α	corrected angle of attack of aircraft, angle between reference body X-axis and stability X-axis, deg or radians
$\dot{\alpha}$	rate of change with time of angle of attack, radians/sec
α_p	maximum positive or negative angle of attack attained in a roll maneuver, deg
β	corrected angle of sideslip, deg or radians
$\dot{\beta}$	rate of change with time of angle of sideslip, radians/sec
δ	control-surface deflection, deg or radians
δ_a	aileron deflection, positive when left aileron is deflected down, deg or radians
δ_{a_β}	rate of change of aileron deflection with sideslip angle
δ_e	elevator deflection, positive when deflected down, deg or radians
δ_r	rudder deflection, positive when deflected to left, deg or radians
δ_{r_β}	rate of change of rudder deflection with sideslip angle
Δ	angle between reference X-axis and plane of spring couple, positive when spring couple is below reference X-axis forward of the center of gravity, deg
ϵ	angle between reference body X-axis and principal X-axis, positive when reference axis is above principal axis at the nose, deg
ζ	ratio of actual damping to critical damping
η	angle of inclination of principal X-axis relative to stability X-axis, positive when principal X-axis is above stability X-axis at the nose, $\alpha - \epsilon$, deg

ρ	mass density of air, slugs/ft^3
τ	time parameter, $\frac{m}{\rho VS}$, sec
μ_l	density parameter, $\frac{m}{\rho Sc}$
ψ,θ,φ	when used with equations correcting for misalinement of instruments, the symbols refer to the misalinement in yaw, pitch, and roll, respectively, relative to the body axes, deg; or, when used with the equations of motion, the symbols refer to displacements in yaw, pitch, and roll, respectively, radians
Φ	phase angle, deg
Φ_d	damping angle, deg
ω_n	undamped natural frequency of aircraft, radians/sec
ω_{n_d}	damped natural frequency of aircraft, radians/sec
Ω	angular rate of rotation of rotating mass of engine, radians/sec

Subscripts:

i	instrument
max	maximum
r	reference axes
s	stability axes

The symbol $|j|$ represents the absolute magnitude of a j quantity and is positive. The phase angle of a vector j relative to another vector k is indicated by the subscript Φ_{jk}. The second subscript is used as the reference. For example, in the expression $\Phi_{\varphi\psi} = -150°$ the roll displacement vector lags the yaw displacement vector by 150°.

TEST TECHNIQUES

The maneuver performed for determining stability derivatives from flight data should be compatible with the requirements of the method of analysis to be employed. Inasmuch as linear theory is used in the determination of derivatives, individual control inputs are used to excite the longitudinal and the lateral motions. Analyses are conducted with various types of control inputs; the simple pulse maneuver in figure 2 is found suitable in general practice. For this maneuver, the airplane is trimmed at the desired angle of attack, altitude, and Mach number, and a free oscillation is initiated by an abrupt pulse. The resulting free-oscillation of the aircraft is allowed to damp with the controls held fixed. With an irreversible control system this is easily accomplished by releasing the controls. Even small inadvertent control inputs during the free-oscillation portion of the maneuver can significantly affect the results.

Most of the flight tests at HSFS are made in 1 g flight at constant Mach number and altitude. Some variations in these quantities are accepted if the resultant change in dynamic pressure is not more than 5 percent. When dynamic-pressure effects are known to be small, tests are made at different base altitudes to determine the variation of airplane characteristics with angle of attack. Similarly, investigations to determine static aeroelastic effects are conducted at different altitudes when angle-of-attack effects are known to be negligible. When flight maneuvers intended specifically for derivative determination are unavailable, the airplane response to random inputs is analyzed to give limited stability data. This is accomplished effectively with the aid of an analog computer. In regions where large Mach number effects exist, tests are conducted at close Mach number intervals with more rigid requirements on constant Mach number and altitude.

The effects of angle of attack and load factor are obtained by performing pulse maneuvers while the airplane is stabilized in an elevated g turn. The application of this technique is limited by the difficulty of performing a good maneuver. Difficulty has been experienced, during the maneuver, in holding the proper bank angle to maintain constant load factor and Mach number. With a conventional control system exceptional piloting skill is required to maintain fixed control during the airplane oscillation at elevated g. The use of the airplane damper as a device for applying a known deflection signal to excite the desired unaugmented airplane oscillation offers a means of improving the quality of the data for 1 g conditions and of obtaining an even greater improvement at elevated g conditions.

The analysis of data of a complete flight program for the determination of stability derivatives of an airplane can be tedious and exacting. The number of computations necessary for an effective analysis of flight data makes it apparent that systematic procedures are helpful. Tabulation forms that include many pertinent flight quantities have proved useful (fig. 3).

MASS CHARACTERISTICS

The airplane mass characteristics--weight, location of the center of gravity, moment of inertia, and inclination of the principal axis--significantly affect airplane motions. Errors in these quantities are reflected directly in the flight-determined derivatives. Weight and horizontal location of the center of gravity are always determined experimentally. Inasmuch as the vertical location of the center of gravity, moments of inertia, and principal-axis location are difficult to determine experimentally,

manufacturer's estimates are usually relied upon. These estimates are generally considered to be of sufficient accuracy for most work involving flight tests. If more precise data are required, they should be determined using experimental techniques.

Weight and Center-of-Gravity Location

The weight and longitudinal position of the center of gravity relative to the horizontal reference line of the airplane for the empty- and gross-weight conditions can easily be obtained by leveling the airplane on suitable scales or electronic weighing cells. The center-of-gravity variation with fuel consumption can usually be defined adequately by weighing the airplane at several fuel levels. In some instances, however, it has been found necessary to account for fuel-tank shape and airplane attitude. The horizontal location of the center of gravity is experimentally obtained at least to within 0.01 mean aerodynamic chord, which is considered adequate for derivative determination.

An accurate knowledge of the vertical location of the center of gravity has not been pertinent to the experimental derivative studies conducted at the High-Speed Flight Station except in the experimental determination of moments of inertia. The vertical center of gravity can be obtained by static or oscillatory techniques. The oscillatory technique consists of changing the equivalent torsional spring constant for the rolling moment-of-inertia tests (fig. 4).

Moments of Inertia

Manufacturer's estimates of the moments of inertia of the airplane are considered adequate for most analysis. However, should the experimental

determination of the inertia be required, because of airplane growth or a need for a more accurate value of inertia, methods are available in references 1 to 3. Schematic representation of typical methods for determining the rolling and pitching moments of inertia of the airplane experimentally are illustrated in figures 4 and 5, respectively. The inertias of rigid airplanes may be determined to within 5 percent or better.

Measuring the inertias of flexible airplanes is more difficult, but has been accomplished to good accuracy for longitudinal moments of inertia (ref. 4).

Difficulties have been encountered due to flexibility in the airplane and in the experimental components used. In one instance the flexibility of a wing that had been considered rigid altered the pivotal point of the oscillations and invalidated the measurements. In another instance, a flexible cable was used as an attach link between the airplane and the restraining spring. The effective spring constant was sufficiently reduced to give erroneous results. Serious errors can also result when knowledge of the center-of-gravity location is inaccurate and when the line of action of the spring at the attach point to the airplane is not perpendicular to the axis of rotation. Generally, the inertia characteristics are determined for no-fuel conditions because fuel sloshing appreciably affects the required oscillatory motion. Theoretical analysis of fuel-sloshing effects has been made (ref. 5), however the theory is approximate.

Inclination of Principal Axis

The inclination of the principal axis of the airplane is one of the more difficult quantities to determine experimentally. As shown in a later section, an error of $1/4°$ in the value of the inclination of the principal

axis can significantly affect the determination of control derivatives. The method of reference 6 is considered to be accurate to 1/6°.

Figures 6 to 8 show the general arrangements of the test setup including the necessary equation for the evaluation of the inclination of the principal axis. Instruments mounted in the airplane measure the roll and yaw rates of the oscillations initiated by a small displacement in yaw. Varying the inclination of the plane of the restoring springs (fig. 6) results in one inclination angle where no rolling is observed and where the formula for determining the inclination of the principal axis is applicable.

Two setups are shown (figs. 7 and 8) but the arrangement of figure 7 is considered to be more convenient and less time consuming. It is essential that the spring provide a pure couple.

The value of the moment of inertia relative to the reference axis I_{Z_r} may be determined from these same tests. The moment of inertia I_{X_r} required in the equation shown in figure 6 must be determined from other tests. Formulas for transferring moments of inertia from one system of axes to another are given in appendix B.

INSTRUMENTATION

Basic to any analysis of flight data is the instrumentation. It is essential to consider each quantity being measured, the sources and probable magnitude of error, and procedures for applying corrections.

Ranges, Sensitivity, and Accuracy

Instruments used for studies of general handling qualities have relatively low sensitivities in order to accommodate the normal flight

range and are employed for approximate evaluation of derivatives in conjunction with these studies. For accurate evaluation of the derivatives, using small disturbance maneuvers, sensitive gyros and accelerometers are installed to supplement or replace those used for the handling qualities studies. The ranges and sensitivities of the instruments and scale factors are usually selected after studying flight-test records of small-perturbation maneuvers performed over a Mach number range during pilot familiarization flights when the airplane is equipped with general purpose flight-test instruments. The increase in sensitivity of any one instrument must be accomplished with discretion, inasmuch as an optimum sensitivity is attained beyond which any increase may simply result in a false sense of accuracy.

Table I shows the characteristics of instruments which are desirable for derivative investigations for one high-performance airplane when the pulsed free-oscillation maneuver is employed. The listed instrument natural frequencies are more than adequate to maintain flat response characteristics during forced portions of the maneuver up to the anticipated maximum frequencies for all recorded quantities.

Phase-Lag Corrections

Since several individually recorded quantities are utilized in the determination of the various derivatives, it is important that the phase-lag characteristics of each recording instrument be taken into consideration. For systems where all the quantities can be recorded on electrical galvanometers, it is generally possible to equalize the individual phase lags by proper choice of the frequency response of the recording system. Where this is not possible, as in the use of certain of the self-recording NASA

instruments, phase-lag corrections must be considered and applied where pertinent.

These corrections are applied by simply shifting the data time scale (ref. 7), as in the determination of control derivatives, or by correcting phase-angle relationships, as in the time-vector method of analysis.

Alinement Accuracy and Misalinement Corrections

As might be expected, it is much less troublesome to obtain correct instrument alinement than to apply misalinement corrections (fig. 9) to flight data.

Rate gyros must be alined to within ±0.2° of correct orientation with relation to all three reference axes. For example, a 3° misalinement of the yaw-rate gyro in pitch changed the sign of the derivative $C_{n_{\delta_a}}$ which had significant effects on the analog-simulated rolling characteristics of the airplane.

Corrections for Location of Instruments

Linear accelerometers.- Although it would be highly desirable to locate linear accelerometers at the center of gravity, this is generally not possible. Therefore, corrections of indicated linear accelerometer readings to the center of gravity of the aircraft must be made using the expressions shown in figure 10. The equations for normal acceleration a_n and transverse acceleration a_t can be linearized and corrections thus simplified by mounting the accelerometers in the plane of symmetry along the X-axis.

Angle-of-attack and sideslip vanes.- Angle-of-attack and sideslip vanes are subject to the effects of upwash, shock waves, and crossflow. Details of these effects are discussed in reference 8. To minimize these effects,

long nose booms are used with the vanes mounted (fig. 11) 1 1/2 fuselage diameters ahead of the nose of the aircraft whenever feasible. Aside from corrections for upwash, shock waves, and crossflow, the indicated vane readings must be corrected for boom-bending effects resulting from aerodynamic and inertia loads. Also, corrections must be applied for angular velocity effects to correct the readings to the center of gravity of the airplane.

METHODS OF ANALYSIS

Of the many methods available for the determination of stability and control derivatives, only a few are simple enough to be practical for a relatively rapid determination of these derivatives. In the following sections some of the methods currently used at the High-Speed Flight Station, including approximate equations, are discussed at some length. Pertinent details regarding the application of the graphical time-vector method are presented in appendix C. Some experience has also been obtained with a number of other detailed methods. Comments on these methods are offered at the conclusion of this section.

On the basis of recent flight experience, it is believed that maximum accuracy is needed in the various control and cross-control derivatives, the static stability derivatives, and the rotary derivative C_{l_p}, since they dominate the basic airplane motions. In lightly damped airplanes the damping derivatives $(C_{m_q} + C_{m_{\dot{\alpha}}})$ and $(C_{n_r} - C_{n_{\dot{\beta}}})$ appear to be of somewhat less consequence; similarly, C_{L_α} and C_{Y_β} are of secondary importance in most stability investigations. Hence less accuracy may be tolerated in these quantities.

Inasmuch as flight-test instruments are referenced to the body axes, it is much less time consuming to analyze for derivatives relative to this system of axes rather than to the stability system of axes. Conversion of derivatives from the body system to the stability system, if required, is accomplished by the equations listed in appendix D.

Basic Data

Application of the simpler equations requires an evaluation of the period and damping, whereas application of the time-vector method requires, in addition, the determination of amplitude and phase relationships. These quantities are obtained from the free-oscillation portion of the pulse maneuver, as illustrated in figure 12. The spacing of the peaks of the oscillatory motions determines the damped natural period, and a comparison of these peaks for the different oscillatory quantities determines their phase relationship. The phase relationships of the pertinent quantities are obtained by an averaging process typified by the table in figure 12(a). The first line lists the time of occurrence of consecutive + and - peaks of the roll rate p. Similarly, the second line lists the + and - peaks of the yaw rate r. The third line lists the time difference of the first two lines in each column. Since the yaw rate is the reference in this instance, the signs in the third line indicate the roll rate is lagging the yaw rate. The values in the third line are averaged and, if need be, converted to phase lag in degrees. It will be noticed that a yawing divergence is evident in the yaw-rate record shown in figure 12. To isolate the oscillatory motions and determine the time to damp of the oscillations, exponential curves are drawn as shown. A semilog plot of the double amplitudes included between the exponential outlines of each motion

establishes the time to damp of the oscillations (fig. 12(b)). A comparison of the plotted double amplitudes of the variables determines the amplitude ratios.

For lightly damped oscillations it is possible to determine the period to within 0.02 second. Good accuracy in damping can be measured for damping ratios less than 0.2. Accuracy of measuring period and damping becomes rather poor for damping ratios greater than about 0.30. Generally, all configurations tested at moderate and high altitudes and without damper augmentation have been rather lightly damped so that free-oscillation methods of analysis can be applied with good accuracy.

The damping ratio ζ, damping angle Φ_d, and undamped natural frequency ω_n are obtained from the following relations

$$\zeta = \sin\left[\tan^{-1}\left(\frac{0.693P}{2\pi T_{1/2}}\right)\right] \tag{1}$$

$$\Phi_d = \tan^{-1}\frac{0.693P}{2\pi T_{1/2}} \tag{2}$$

$$\omega_n^2 = \omega_{n_d}^2 + \omega_n^2\zeta^2 = \left(\frac{2\pi}{P}\right)^2 + \left(\frac{0.693}{T_{1/2}}\right)^2 \tag{3}$$

Longitudinal Stability and Control Derivatives

The nature of the input and the ensuing free oscillations of the longitudinal pulse maneuver permit the use of relatively simple methods of analysis. These simple methods give results comparable to those from the more complicated methods investigated. Only the relatively simple methods are discussed, and only data from these methods are presented.

Control effectiveness $C_{m_{\delta_e}}$.- The control-effectiveness derivatives are determined from the initial portion, approximately 0.2 second, of a rapid pulse maneuver (fig. 13). During this part of the maneuver the airplane response is almost entirely pitching acceleration with the result that

$$C_{m_{\delta_e}} \approx \frac{I_Y \dot{q}}{\bar{q}S\bar{c}\,\delta_e} \tag{4}$$

Pulses applied at slower rates, and thus extending over a longer time interval, may require the inclusion of pitch damping and angle-of-attack terms in the equation.

Analysis by this method requires instruments with flat response characteristics extending to relatively high frequencies (8 cycles per second) and also requires the application of instrument phase-lag corrections previously discussed. By checking the characteristics of the instruments being used, it has been found that the time difference in peak values of control input and pitching accelerations is a result of instrument lag (fig. 13).

Utilizing this method of analysis it is believed that the control effectiveness can be obtained to within 10 percent; the error is primarily attributable to readability of the peak values of control input and acceleration.

Static stability derivative C_{m_α}.- On the basis of the short-period form of the linearized longitudinal equations of appendix A, the following equation may be obtained from the longitudinal characteristic equation

$$C_{m_\alpha} \approx -\frac{I_Y}{\bar{q}S\bar{c}}\omega_n^2 \tag{5}$$

This equation neglects the term $\frac{1}{4\mu_l} C_{m_q} C_{L_\alpha}$ which has been found to be only 3 to 5 percent of the total. Thus an acceptable value for C_{m_α} can be obtained by simply using the frequency term.

Lift-curve slope C_{L_α}.- From the free oscillation of the airplane with the controls fixed the variation of normal-force coefficient with angle of attack may be evaluated as

$$C_{N_\alpha} \approx \frac{W}{\bar{q}S} \frac{|a_n|}{|\alpha|} = C_{L_t} \frac{|a_n|}{|\alpha|} \tag{6}$$

This expression neglects the pitching-velocity and angle-of-attack-rate terms (see appendix A) of the normal-force equation, but these terms have been found to be negligible. This derivative C_{N_α} may be converted to lift-curve slope by an approximation of the derivative form of the equation

$$C_L = C_N - C_A \sin \alpha + \frac{T}{\bar{q}S} \sin \alpha \tag{7}$$

Since the C_A and the T terms are usually negligibly small relative to C_N at small angles of attack

$$C_{L_\alpha} \approx C_{N_\alpha} \tag{8}$$

Should the angle-of-attack records be unavailable and pitch-rate records available, $\frac{|a_n|}{|\alpha|}$ may be obtained from $\frac{|a_n|}{|q|}$ by using vector principles. A typical solution is included as figure 14.

Damping in pitch $(C_{m_q} + C_{m_{\dot{\alpha}}})$.- From the airplane characteristics equation, the longitudinal damping derivative may be evaluated as

$$(C_{m_q} + C_{m_{\dot{\alpha}}}) = \frac{2I_Y}{m\bar{c}^2} \left[C_{L_\alpha} - 4\tau \left(\frac{0.693}{T_{1/2}} \right) \right] \tag{9}$$

This derivative can be determined to reasonable accuracy for damping ratios up to about 0.2, but to less accuracy at higher damping ratios. The accuracy in determining $(C_{m_q} + C_{m_{\dot{\alpha}}})$ is affected by taking the small difference between two relatively large numbers. Small errors in either of these large numbers are amplified in the determined derivative.

Representative results.- Using the methods of analysis discussed, longitudinal derivatives have been evaluated for a representative contemporary test airplane and are presented in figure 15. These data are typical of those that can be obtained from good flight techniques and careful application of the methods of analysis.

The maximum deviation from the faired value in the primary derivatives, which occurs in the control-effectiveness derivative $C_{m_{\delta_e}}$, is about 20 percent. In the static stability derivative C_{m_α} the deviation is only 10 percent. Deviations of this magnitude occur in only 5 percent of the data analyzed.

It is customary to perform maneuvers at closer Mach number intervals in the transonic region than in other regions to establish the extent of any abrupt changes of the derivatives. Such an abrupt change is well defined for C_{m_α} in figure 15.

Included in figure 15 are the results of good and bad practices of analog studies performed to ascertain the validity of the flight-determined derivatives. Actual flight-control input motions were used in the analog studies. At Mach numbers of 0.94 and 1.6, the overlays used in comparing simulated and flight time histories were based on indicated time histories corrected to the center of gravity of the airplane and for phase-lag errors of the instruments. At a Mach number of 1.27, the overlay for

comparing analog and flight time history did not include any corrections to the indicated flight data. Where the simulated time history did not agree with the overlay, the stability derivatives determined from flight data were altered until the agreement was optimum. At a Mach number of 1.27, the results of the analog study are erroneous because of the inadequate attention to corrections of indicated time history in making the overlay. Figure 16 shows a comparison of the actual flight and simulated motions at a Mach number of 1.6. The agreement is considered good and substantiates the fact that the flight derivatives adequately describe the test airplane at the test condition shown.

Lateral Stability and Control Derivatives

The lateral stability and control derivatives are not determined as readily and reliably by use of approximate equations as are the longitudinal derivatives because of the complex behavior of the airplane. The following discussion considers the various methods used at the High-Speed Flight Station.

Control effectiveness.- The basic procedures for determining lateral and directional control effectiveness are similar to those previously discussed. However, the expressions for lateral-directional control effectiveness are complicated by the need to account for the possible influence of the inclination of the principal axis as well as the aerodynamic terms. Tests with one conventional high-performance airplane utilizing a rapid control pulse or step maneuver show that the directional-control derivative $C_{n_{\delta_r}}$ can be determined to good accuracy considering only the inertia term.

For example

$$C_{n_{\delta_r}} = \left[\frac{I_Z}{\bar{q}Sb}\dot{r} - \frac{I_{XZ}}{\bar{q}Sb}\dot{p} - (C_{n_r} - C_{n_{\dot{\beta}}})\frac{rb}{2V} - C_{n_p}\frac{pb}{2V} - C_{n_\beta}\beta\right]\frac{1}{\delta_r} \qquad (10)$$

$$100 = \quad 98 \quad - \quad 0 \quad + \quad 2 \quad - \quad 0 \quad - \quad 0$$

where the magnitudes of the individual terms are given as percentages of the answer. It should not be precluded that the inertia term is the only term which will be significant in determining $C_{n_{\delta_r}}$ for other aircraft. For the roll-control derivative $C_{l_{\delta_a}}$, consideration must be given to the aerodynamic derivative terms. For example

$$C_{l_{\delta_a}} = \left[\frac{I_X}{\bar{q}Sb}\dot{p} - \frac{I_{XZ}}{\bar{q}Sb}\dot{r} - C_{l_p}\frac{pb}{2V} - C_{l_r}\frac{rb}{2V} - C_{l_\beta}\beta\right]\frac{1}{\delta_a}$$

$$100 = \quad 73 \quad - \quad 4 \quad + \quad 31 \quad - \quad 0 \quad - \quad 0$$

The cross-control derivatives $C_{n_{\delta_a}}$ and $C_{l_{\delta_r}}$ can be evaluated using equations (10) and (11), respectively. The cross-control derivatives are usually of smaller magnitude and are therefore more difficult to determine. Consideration must be given to all the terms of the equation as is shown in the following example for the analysis for $C_{n_{\delta_a}}$. The flight quantities were obtained from the records as shown in figure 17. The time difference in the peaks of the control input and the accelerations is due to phase lags of the instruments. The acceleration and angular rate records and the sideslip record have practically the correct phase relationship with respect to each other in this instance. Following

are the magnitudes of the individual terms as percentages of the answer

$$C_{n_{\delta_a}} = \left[\frac{I_Z}{\bar{q}Sb}\dot{r} - \frac{I_{XZ}}{\bar{q}Sb}\dot{p} - (C_{n_r} - C_{n_{\dot{\beta}}})\frac{rb}{2V} - C_{n_p}\frac{pb}{2V} - C_{n_\beta}\beta\right]\frac{1}{\delta_a} \qquad (12)$$

$$100 = 206 - 141 + 10 + 9 + 16$$

An error in principal-axis inclination is also particularly significant in determining $C_{n_{\delta_a}}$. For instance in this example an error of 1/4° in the inclination of principal axis (3°) would result in an error of 12 percent in $C_{n_{\delta_a}}$.

Directional-stability derivative C_{n_β}.- Since the static-directional-stability derivative is one of primary importance, good accuracy is required in its measurement. Many methods have been used for evaluating this derivative, and a comparison of typical results is included in figure 18. The results as obtained by the vector method (appendix C) are considered to be accurate to within 10 percent and are used as a basis for comparison.

Simplest of these methods is the frequency dependent approximation where

$$C_{n_\beta} = \frac{I_Z}{\bar{q}Sb}\omega_n^2 \qquad (13)$$

Results from this equation (fig. 18) compare well with the more complete methods at flight conditions where angle of attack and dihedral effects are small. At low indicated airspeeds where these effects are not small, the discrepancy can be 50 percent or more depending on the mass characteristics and the aerodynamics of the individual airplane.

The simple equation can be modified to account for C_{l_β} effects as follows

$$C_{n_\beta} = \frac{I_Z}{\bar{q}Sb}\omega_n^2 - \frac{I_{XZ}}{I_X}C_{l_\beta} + \alpha\frac{I_Z}{I_X}C_{l_\beta} \tag{14}$$

This method relies on wind-tunnel data, theory, or flight values for C_{l_β} and has given satisfactory results except for configurations with high roll-to-yaw ratios. In general, this equation shows better agreement with the more comprehensive methods throughout the Mach number range.

Values of C_{n_β} have also been obtained from steady sideslip maneuvers using the expression

$$C_{n_\beta} = -\left(C_{n_{\delta_r}}\delta_{r_\beta} + C_{n_{\delta_a}}\delta_{a_\beta}\right) \tag{15}$$

Unreliable determination of the control derivatives has limited the use of this equation. Also the inability to obtain sufficient sideslip angle at supersonic conditions makes accurate determination of the apparent stability parameters δ_{r_β} and δ_{a_β} difficult. The results obtained from equation (15) show poor agreement with the other methods, particularly in the supersonic speed range (fig. 18).

Application of these methods for obtaining C_{n_β} has led to a logical approach for the evaluation of this derivative. For configurations with known low values of C_{l_β} at low angles of attack the simple frequency dependent equation for C_{n_β} is usually adequate. Flight conditions at high angles of attack require more complete equations. Still more comprehensive methods, such as the time-vector method, should be used as a check on the validity of the more approximate methods at representative test conditions.

Effective dihedral C_{l_β}.- The dihedral effect can be evaluated from both static and dynamic maneuvers. From steady sideslip

$$C_{l_\beta} = -\left(C_{l_{\delta_r}}\delta r_\beta + C_{l_{\delta_a}}\delta a_\beta\right) \tag{16}$$

The limitations previously discussed for a similar expression for C_{n_β} (equation (15)) also apply for equation (16). For most investigations C_{l_β} is derived by the time-vector solution of the rolling-moment equation.

A comparison of C_{l_β} determined by equation (16) and the time-vector method is shown in figure 19. At low Mach numbers the results from equation (16) compare favorably with the time-vector results. At high Mach numbers a large discrepancy exists between the two methods. Even though C_{l_β} is not one of the derivatives most accurately determined by the time-vector method, the vector method is the most practical means available for evaluating this derivative.

Damping derivatives C_{l_p}, $(C_{n_r} - C_{n_{\dot\beta}})$.- Approximate equations for determining C_{l_p} and $(C_{n_r} - C_{n_{\dot\beta}})$ are

$$C_{l_p} = -C_{l_{\delta_a}}\left(\delta_a \Big/ \frac{pb}{2V}\right) \tag{17}$$

$$(C_{n_r} - C_{n_{\dot\beta}}) = \frac{-2I_Z}{b^2}\left(\frac{2\pi V}{\bar{q}ST_{1/2}} + \frac{1}{m}C_{Y_\beta}\right) \tag{18}$$

In determining C_{l_p} by equation (17), the factor $\left(\delta_a \Big/ \frac{pb}{2V}\right)$ is obtained from aileron rolls and the control effectiveness is determined as previously discussed. Equation (17) often is considerably in error because of adverse yaw coupled with large dihedral effect and is not recommended for general use. This derivative may be determined with better accuracy by the time-vector method (appendix C).

The determination of $(C_{n_r} - C_{n_{\dot{\beta}}})$ by equation (18) has provided reasonable approximations for low angle-of-attack conditions. Results were poor at high angle of attack. This derivative is also a product of the time-vector solution of the yawing-moment equation (appendix C); however, the accuracy is subject to relatively large errors because of its sensitivity to small phase-angle errors and the assumed values of C_{n_p} used in the solution.

Side-force derivative C_{Y_β}.- The side-force derivative is determined by an equation which parallels the longitudinal equation for C_{N_α}

$$C_{Y_\beta} \approx -\frac{W}{\bar{q}S}\frac{|a_t|}{|\beta|} = -C_{L_t}\frac{|a_t|}{|\beta|} \tag{19}$$

The amplitude ratio $\frac{|a_t|}{|\beta|}$ is obtained from flight records which have been corrected for such factors as instrument location. Where β records are not usable or are unavailable, the ratio may be obtained by time-vector methods as shown in figure 20.

Representative results.- A typical set of lateral stability and control derivatives is presented in figure 21. The stability and damping derivatives were obtained by the time-vector method, whereas the control derivatives were calculated by equations (10) to (12).

It is felt that for most quantities the number of test points shown could not have been substantially reduced and still define the curves adequately. The analog was used as a check on the validity of the flight-determined derivatives and in most instances only minor changes to the flight-determined derivatives were required to obtain an optimum match between the flight and calculated motions such as typified in figure 22. It should be noted that the analog matching technique is not completely

satisfactory inasmuch as the solution is not necessarily unique. However, the correlation shown was the result of systematic variations of the flight-determined derivatives and afforded the best comparison of calculated and flight time histories.

Discussion of Other Methods

As mentioned previously, the time-vector method requires the assumption of some derivatives. A number of methods have been proposed for the comprehensive determination of derivatives without requiring such assumptions. Some of these methods have been applied successfully at the High-Speed Flight Station; others have not been successful. In the following paragraphs comments are offered on a number of such derivative methods.

Klawans' method.- This method (ref. 9), based on the time-vector principles and the time plane, utilizes data of the spiral, roll-subsidence, and Dutch roll modes for determining the lateral derivatives. The method equates the real and imaginary quantities in each of the three equations of motion, thus providing six equations from the Dutch roll mode. The spiral and roll-subsidence modes provide additional equations. The method requires the same basic analysis of free-oscillation data as required by the graphical time-vector method (amplitude ratios, phase angles, damping, and natural frequency). It also requires analysis of the spiral or roll-subsidence amplitude ratios, or both, and roots for the evaluation of C_{n_p} and C_{l_r}. The method is simple and direct. The deterrent to its use is the difficulty of specifying flight techniques which will provide data from which spiral and roll-subsidence amplitude ratios and roots can be obtained. If C_{n_p} and C_{l_r} are estimated, the

method becomes the mathematical equivalent of the graphical time-vector approach.

Transfer-function-equation method.- The method of reference 10 involves the use of simplified transfer-function equations that best describe the various measured frequency responses. The transfer coefficients are evaluated by a curve-fitting process involving the use of templates and an analog computer. The pertinent stability derivatives are then evaluated from the transfer coefficients. The derivatives determined include the important stability and damping derivatives and the control derivatives $C_{m_{\delta_e}}$, $C_{n_{\delta_r}}$, and $C_{l_{\delta_a}}$. The method provides reasonably good results but entails a considerable amount of work. However, when the airplane is heavily damped, or when frequency-response data are required for other purposes, the method may be used to advantage. Practical use of this method requires both digital and analog computing equipment.

Frequency-response method.- The method of reference 11 replaces the time plane with the frequency plane. Amplitude ratios and phase relationships of airplane response to control input from frequency-response analysis provide real and imaginary quantities. These complex quantities substituted in the three equations of motion result in six equations. Selection of data at discrete frequencies provides as many simultaneous equations as necessary for a least-squares process to determine the derivatives. The method is simple in theory and has produced good results. Considerable care, work, and time are involved in the application, and some experience is necessary in the selection of discrete frequencies. Automatic data-reduction equipment would greatly expedite the frequency-response analysis and would be useful for the other computations required.

Least-squaring of the equations of motion.- A logical and simple method for determining derivatives from flight data is the least-squares method. Flight quantities at discrete times are substituted into the equations of motion. Many more data points are selected than the number of unknowns, and a least-squares process is applied for evaluating the unknown derivatives. The use of better-conditioned maneuvers and more specialized instrumentation may make the method feasible. It appears that the accuracy required is greater than that required by most methods of analysis.

APPLICATIONS OF FLIGHT DERIVATIVES

No paper on flight derivatives would be complete without some discussion of the manner in which flight derivatives are applied.

Flight Guidance

For several years a considerable effort has been expended at the High-Speed Flight Station in flight and simulator studies relating to the inertia-coupling problem. Because of the complex nature of the motions, guidance of the flight program by use of analog computations is highly desirable. In a roll investigation of this type a small increase in aileron deflection can produce large effects on airplane motions, and it has been graphically demonstrated on several occasions that flight guidance based on linear extrapolation of flight data at small aileron deflections can be highly misleading and dangerous. Figure 23 shows a representative comparison of the measured excursions in angle of attack and sideslip angle obtained in 360° rolls with those predicted using flight-determined derivatives. The good agreement shown has been demonstrated in most

instances in which flight-determined derivatives have formed the basis of the calculations, and consequently, the use of such guidance in flight planning has proved invaluable. The use of wind-tunnel and theoretical derivatives in analog studies has not been nearly so successful.

Because the directional stability of most aircraft decreases at supersonic speed there usually exists a critical need for flight guidance to avoid directional divergence near design Mach number. Inasmuch as this decay in directional stability is often even more evident as angle of attack is increased, the analysis must of necessity include accelerated flight conditions. Flight-determined directional-stability derivative C_{n_β} is obtained from pulse maneuvers in a cautious buildup program.

Jet-exhaust effects have also been known to affect the directional stability appreciably, and these effects are difficult to simulate in the wind tunnel. Figure 24 demonstrates the large detrimental effect of the jet exhaust of a rocket engine on one airplane in the supersonic region. The magnitude of this effect was unusually large in this instance. At least a cursory check of power effects is made in flight on rocket airplanes.

Verification of Wind-Tunnel Data and Theory

The designer has used the results of flight tests as one means of verifying theory as well as small-scale wind-tunnel data. Figure 25 shows a comparison of flight and wind-tunnel directional-stability characteristics. The results indicate that when the basic rigid tunnel data were corrected for aeroelasticity and air-intake flow, fairly good correlation existed with the flight data.

When first-order aeroelastic corrections are applied to rigid wind-tunnel data, it has been found that lift-curve slope and lateral-force derivatives agree within about 5 percent of flight results. The correlation of tunnel and flight static-stability derivatives C_{m_α} and C_{n_β} in the low angle-of-attack range is generally within about 10 percent. Flight control effectiveness is usually within 10 to 20 percent of the wind-tunnel value, and damping and dihedral effect can be expected to agree within about 20 percent. The differences shown result from uncertainties in the mass characteristics as well as from the analysis of the data.

CONCLUDING REMARKS

A comprehensive discussion of the various factors affecting the determination of stability and control derivatives from flight data has been presented based on the experience of the NASA High-Speed Flight Station. Factors relating to test techniques, determination of mass characteristics, instrumentation, and methods of analysis were discussed.

The pulse maneuver has been found generally adequate in exciting the motions required for stability-derivative analysis if adequate instrumentation sensitivity and alinement are provided.

For most longitudinal-stability-derivative analyses simple equations utilizing period and damping have been found to be as satisfactory as more comprehensive methods. The graphical time-vector method has been the basis of lateral-derivative analysis at the High-Speed Flight Station, although simple approximate methods can be useful if applied with caution. Control effectiveness has been generally obtained by relating the

peak acceleration to the rapid control input. Consideration must be given to aerodynamic contributions if reasonable accuracy is to be realized.

Because of the many factors involved in the determination of accuracy requirements, it is believed that the primary stability and control derivatives are probably accurate to within 10 to 25 percent, depending upon the specific derivative. Static-stability derivatives at low angle of attack show the greatest accuracy.

Present instrumentation and methods of analysis are adequate for the extraction of derivatives from flight data for use in flight-guidance simulator studies and in detecting characteristics which have not been predicted in the wind tunnel.

APPENDIX A

EQUATIONS OF MOTION FOR FIVE-DEGREE-OF-FREEDOM BODY SYSTEM OF AXES

Equations for the nonlinear form are:

Velocity components

$u = V \cos \alpha \cos \beta$

$v = V \sin \beta$ $\qquad \dot{v} = V\dot{\beta} \cos \beta$

$w = V \sin \alpha$ $\qquad \dot{w} = V\dot{\alpha} \cos \alpha$

Force equations

(Resultant thrust of engine is assumed to lie in plane of symmetry parallel to body axes.)

$$a_n = - (\dot{w} - uq + vp - g \cos \theta \cos \varphi) \, 1/g$$

$$a_t = (\dot{v} - wp + ur - g \cos \theta \sin \varphi + g \sin \theta \sin \beta) \, 1/g$$

$$Wa_n = \left(C_{N_\alpha}\alpha + C_{N_q} \frac{q\bar{c}}{2V} + C_{N_{\dot{\alpha}}} \frac{\dot{\alpha}\bar{c}}{2V} + C_{N_\delta}\delta\right)\bar{q}S$$

$$Wa_t = \left(C_{Y_\beta}\beta + C_{Y_p} \frac{pb}{2V} + C_{Y_r} \frac{rb}{2V} + C_{Y_{\dot{\beta}}} \frac{\dot{\beta}b}{2V} + C_{Y_\delta}\delta\right)\bar{q}S$$

Moment equations

$$I_Y\dot{q} - (I_Z - I_X)pr - I_{XZ}(r^2 - p^2) + I_{X_e}\Omega r =$$

$$\left(C_{m_\alpha}\alpha + C_{m_q} \frac{q\bar{c}}{2V} + C_{m_{\dot{\alpha}}} \frac{\dot{\alpha}\bar{c}}{2V} + C_{m_\beta}\beta + C_{m_\delta}\delta\right)\bar{q}S\bar{c} + Tz_e$$

$$I_X\dot{p} + (I_Z - I_Y)qr - I_{XZ}(\dot{r} + pq) =$$

$$\left(C_{l_\beta}\beta + C_{l_p} \frac{pb}{2V} + C_{l_r} \frac{rb}{2V} + C_{l_{\dot{\beta}}} \frac{\dot{\beta}b}{2V} + C_{l_\delta}\delta\right)\bar{q}Sb$$

$$I_Z\dot{r} + (I_Y - I_X)pq - I_{XZ}(\dot{p} - qr) - I_{X_e}\Omega q =$$

$$\left(C_{n_\beta}\beta + C_{n_p} \frac{pb}{2V} + C_{n_r} \frac{rb}{2V} + C_{n_{\dot{\beta}}} \frac{\dot{\beta}b}{2V} + C_{n_\delta}\delta\right)\bar{q}Sb$$

APPENDIX B

CONVERSION OF MOMENTS OF INERTIA FROM ONE SET OF AXES TO ANOTHER

Formulas for transferring moments of inertia from body axes to stability:

$$I_{X_s} = 1/2(I_X + I_Z) - 1/2(I_Z - I_X)\cos 2\alpha - I_{XZ} \sin 2\alpha$$

$$I_{Z_s} = 1/2(I_Z + I_X) + 1/2(I_Z - I_X)\cos 2\alpha + I_{XZ} \sin 2\alpha$$

$$I_{Y_s} = I_Y$$

$$I_{X_s Z_s} = 1/2(I_X - I_Z)\sin 2\alpha + I_{XZ} \cos 2\alpha$$

Formulas for transferring moments of inertia from stability axes to body:

$$I_X = 1/2(I_{X_s} + I_{Z_s}) - 1/2(I_{Z_s} - I_{X_s})\cos 2\alpha + I_{X_s Z_s} \sin 2\alpha$$

$$I_Z = 1/2(I_{Z_s} + I_{X_s}) + 1/2(I_{Z_s} - I_{X_s})\cos 2\alpha - I_{X_s Z_s} \sin 2\alpha$$

$$I_Y = I_{Y_s}$$

$$I_{XZ} = I_{X_s Z_s} \cos 2\alpha - 1/2(I_{X_s} - I_{Z_s})\sin 2\alpha$$

Formulas for transferring moments of inertia from the principal axes to stability:

$$I_{X_s} = I_{X_0} \cos^2\eta + I_{Z_0} \sin^2\eta$$

$$I_{Z_s} = I_{Z_0} \cos^2\eta + I_{X_0} \sin^2\eta$$

$$I_{Y_s} = I_{Y_0}$$

$$I_{X_s Z_s} = 1/2(I_{X_0} - I_{Z_0})\sin 2\eta$$

Equations for the linear form are:

Velocity components

$u \approx V$

$v \approx V\beta$ $\qquad\qquad$ $\dot{v} \approx V\dot{\beta}$

$w \approx V\alpha$ $\qquad\qquad$ $\dot{w} \approx V\dot{\alpha}$

Force equations

$$a_n = -(\dot{w} - uq - g)\, 1/g$$

$$a_t = (\dot{v} - wp + ur - g\varphi)\, 1/g$$

$$Wa_n = \left(C_{N_\alpha}\alpha + C_{N_q}\frac{q\bar{c}}{2V} + C_{N_{\dot{\alpha}}}\frac{\dot{\alpha}\bar{c}}{2V} + C_{N_\delta}\delta\right)\bar{q}S$$

$$Wa_t = \left(C_{Y_\beta}\beta + C_{Y_p}\frac{pb}{2V} + C_{Y_r}\frac{rb}{2V} + C_{Y_{\dot{\beta}}}\frac{\dot{\beta}b}{2V} + C_{Y_\delta}\delta\right)\bar{q}S$$

Note: -w assumed constant

Moment equations

$$I_Y\dot{q} = \left(C_{m_\alpha}\alpha + C_{m_q}\frac{q\bar{c}}{2V} + C_{m_{\dot{\alpha}}}\frac{\dot{\alpha}c}{2V} + C_{m_\delta}\delta\right)\bar{q}S\bar{c} + Tz_e$$

$$I_X\dot{p} - I_{XZ}\dot{r} = \left(C_{l_\beta}\beta + C_{l_p}\frac{pb}{2V} + C_{l_r}\frac{rb}{2V} + C_{l_{\dot{\beta}}}\frac{\dot{\beta}b}{2V} + C_{l_\delta}\delta\right)\bar{q}Sb$$

$$I_Z\dot{r} - I_{XZ}\dot{p} = \left(C_{n_\beta}\beta + C_{n_p}\frac{pb}{2V} + C_{n_r}\frac{rb}{2V} + C_{n_{\dot{\beta}}}\frac{\dot{\beta}b}{2V} + C_{n_\delta}\delta\right)\bar{q}Sb$$

APPENDIX C

Time-Vector Method

The graphical time-vector method (refs. 12 to 14) is currently the method most commonly used by the High-Speed Flight Station for the determination of lateral-stability derivatives. One advantage of the method is that the procedure is manual, and the analyst is afforded a graphical presentation of various factors affecting the solution. Another advantage is that it is possible to obtain solutions when the β-vane records are unavailable or when it is desired to avoid applying corrections to these records. Bypassing of the β records is accomplished by setting up the various pertinent amplitude ratios and phase angles with the yaw rate vector as the base. The vector polygon of the transverse acceleration equation shown in figure 26(a) is an essential part of the overall solution inasmuch as the amplitude ratio $\left|\frac{\beta}{r}\right|$ and the phase angle $\Phi_{\beta r}$ determined from figure 26(a) are employed in the moment polygons. The phase angle is used in the orientation of the β vector in relation to the r vector and provides a more accurate value than can generally be obtained from the flight records directly. The amplitude ratio $\left|\frac{\beta}{r}\right|$ is used to extract C_{n_β} and C_{l_β} from the determined values of $C_{n_\beta}\left|\frac{\beta}{r}\right|$ and $C_{l_\beta}\left|\frac{\beta}{r}\right|$ in figures 26(b) and (c), respectively.

The method is not without its disadvantages. One disadvantage is that the development is required of a definite technique on the part of the analyst to minimize what would otherwise constitute a rather time-consuming and tedious effort to obtain a consistent set of results.

Another disadvantage is that only two of the three derivatives in each of the lateral moment equations may be determined by means of the

Formulas for transferring moments of inertia from principal axes to body:

$$I_X = 1/2(I_{X_0} + I_{Z_0}) + 1/2(I_{X_0} - I_{Z_0})\cos 2\epsilon$$

$$I_Z = 1/2(I_{Z_0} + I_{X_0}) + 1/2(I_{Z_0} - I_{X_0})\cos 2\epsilon$$

$$I_Y = I_{Y_0}$$

$$I_{XZ} = 1/2(I_{Z_0} - I_{X_0})\sin 2\epsilon$$

APPENDIX D

CONVERSION EQUATIONS TO TRANSFER STABILITY DERIVATIVES FROM ONE SYSTEM OF AXES TO ANOTHER

Formulas for transferring stability derivatives from stability to body axes:

$$C_{n_\beta} = C_{n_{\beta_s}} \cos\alpha + C_{l_{\beta_s}} \sin\alpha$$

$$C_{l_\beta} = C_{l_{\beta_s}} \cos\alpha - C_{n_{\beta_s}} \sin\alpha$$

$$C_{n_r} \cdot C_{n_{\dot\beta}} = \left(C_{n_{r_s}} - C_{n_{\dot\beta_s}}\right) \cos^2\alpha + C_{l_{p_s}} \sin^2\alpha + \left(C_{n_{p_s}} + C_{l_{r_s}} - C_{l_{\dot\beta_s}}\right) \sin\alpha \cos\alpha$$

$$C_{l_r} - C_{l_{\dot\beta}} = \left(C_{l_{r_s}} - C_{l_{\dot\beta_s}}\right)\cos^2\alpha - C_{n_{p_s}} \sin^2\alpha - \left(C_{n_{r_s}} - C_{n_{\dot\beta_s}} - C_{l_{p_s}}\right) \sin\alpha \cos\alpha$$

$$C_{n_p} = C_{n_{p_s}} \cos^2\alpha - \left(C_{l_{r_s}} - C_{l_{\dot\beta_s}}\right) \sin^2\alpha - \left(C_{n_{r_s}} - C_{n_{\dot\beta_s}} - C_{l_{p_s}}\right) \sin\alpha \cos\alpha$$

$$C_{l_p} = C_{l_{p_s}} \cos^2\alpha + \left(C_{n_{r_s}} - C_{n_{\dot\beta_s}}\right) \sin^2\alpha - \left(C_{n_{p_s}} + C_{l_{r_s}} - C_{l_{\dot\beta_s}}\right) \sin\alpha \cos\alpha$$

Formulas for transferring stability derivatives from body to stability axes:

$$C_{n_{\beta_s}} = C_{n_\beta} \cos\alpha - C_{l_\beta} \sin\alpha$$

$$C_{l_{\beta_s}} = C_{l_\beta} \cos\alpha + C_{n_\beta} \sin\alpha$$

vector diagram, thus necessitating an estimate or a wind-tunnel value of one of the derivatives in each of the equations. Since the C_{n_p} and C_{l_r} terms in the vector diagrams (figs. 26(a) and (b)) are the smallest vectors, it is customary to estimate these quantities. The errors in the estimated values of C_{n_p} will affect $(C_{n_r} - C_{n_{\dot{\beta}}})$ primarily; the errors in C_{l_r} will affect C_{l_p} primarily. The best accuracy in determining C_{n_β} and $(C_{n_r} - C_{n_{\dot{\beta}}})$ is obtained when the roll-to-yaw ratio is small; at this time the influence of C_{n_p} is relatively small. When the roll-to-yaw ratio is large, it may be advantageous to estimate $(C_{n_r} - C_{n_{\dot{\beta}}})$ and attempt to solve for C_{n_p}. For low angles of attack $(C_{n_r} - C_{n_{\dot{\beta}}})$ may be estimated by using equation (18). The best accuracy in determining C_{l_β} and C_{l_p} is obtained when the roll-to-yaw ratio is large. At this time the influence of C_{l_r} is relatively small. In either case, the static derivatives C_{n_β} and C_{l_β} are determined more accurately than the rotary derivatives $(C_{n_r} - C_{n_{\dot{\beta}}})$ and C_{l_p}.

A limitation in the application of the method is the inability to work with records of heavily damped aircraft. The accuracy of analysis becomes rather poor for damping ratios greater than 0.3. Although a good approximation of the damping ratio for heavily damped aircraft may be obtained by comparing flight records with records of heavily damped motions--the damping ratio of which is known--it becomes difficult to draw accurately the exponential envelopes of the oscillatory motions to obtain reliable values of amplitude ratios.

$$C_{n_{r_s}} - C_{n_{\dot{\beta}_s}} = (C_{n_r} - C_{n_{\dot{\beta}}})\cos^2\alpha + C_{l_p}\sin^2\alpha -$$

$$(C_{l_r} - C_{l_{\dot{\beta}}} - C_{n_p})\sin\alpha\cos\alpha$$

$$C_{l_{r_s}} - C_{l_{\dot{\beta}_s}} = (C_{l_r} - C_{l_{\dot{\beta}}})\cos^2\alpha - C_{n_p}\sin^2\alpha +$$

$$(C_{n_r} - C_{n_{\dot{\beta}}} - C_{l_p})\sin\alpha\cos\alpha$$

$$C_{n_{p_s}} = C_{n_p}\cos^2\alpha - (C_{l_r} - C_{l_{\dot{\beta}}})\sin^2\alpha + (C_{n_r} - C_{n_{\dot{\beta}}} - C_{l_p})\sin\alpha\cos\alpha$$

$$C_{l_{p_s}} = C_{l_p}\cos^2\alpha + (C_{n_r} - C_{n_{\dot{\beta}}})\sin^2\alpha + (C_{l_r} - C_{l_{\dot{\beta}}} + C_{n_p})\sin\alpha\cos\alpha$$

REFERENCES

1. Turner, Howard L.: Measurement of the Moments of Inertia of an Airplane by a Simplified Method. NACA TN 2201, 1950.

2. Notess, Charles B., and Woodard, Claude R.: An Investigation of the Experimental Determination of Aircraft Inertia Characteristics. WADC Tech. Rep. 53-207, July 1953.

3. Woodard, Claude R.: Handbook of Instructions for Experimentally Determining the Moments of Inertia and Product of Inertia of Aircraft by the Spring Oscillation Methods. WADC Tech. Rep. 55-415, June 1955.

4. Cole, Henry A., Jr., and Bennion, Frances L.: Measurement of the Longitudinal Moment of Inertia of a Flexible Airplane. NACA TN 3870, 1956.

5. Schy, Albert A.: A Theoretical Analysis of the Effects of Fuel Motion on Airplane Dynamics. NACA TN 2280, 1951.

6. Boucher, Robert W., Rich, Drexel A., Crane, Harold L., and Matheny, Cloyce E.: A Method for Measuring the Product of Inertia and the Inclination of the Principal Longitudinal Axis of Inertia of an Airplane. NACA TN 3084, 1954.

7. Seckel, Edward: Systematic Errors. Vol. IV of AGARD Flight Test Manual, Pt. IVA, North Atlantic Treaty Organization, pp. IVA:1-IVA:8.

8. Beeler, De E., Bellman, Donald R., and Saltzman, Edwin J.: Flight Techniques for Determining Airplane Drag at High Mach Numbers. NACA TN 3821, 1956.

9. Klawans, Bernard B., and White, Jack A.: A Method Utilizing Data on the Spiral, Roll-Subsidence, and Dutch Roll Modes for Determining Lateral Stability Derivatives From Flight Measurements. NACA TN 4066, 1957.

10. Triplett, William C., Brown, Stuart C., and Smith, G. Allan: The Dynamic-Response Characteristics of a 35° Swept-Wing Airplane As Determined From Flight Measurements. NACA Rep. 1250, 1955. (Supersedes NACA RM A51G27 by Triplett and Smith and RM A52I17 by Triplett and Brown.)

11. Donegan, James J., Robinson, Samuel W., Jr., and Gates, Ordway B., Jr.: Determination of Lateral-Stability Derivatives and Transfer-Function Coefficients From Frequency-Response Data for Lateral Motions. NACA TN 3083, 1954.

12. Breuhaus, W. O.: Resumé of the Time Vector Method as a Means for Analyzing Aircraft Stability Problems. WADC Tech. Rep. 52-299 (Contract No. AF33(038)-20659 RDO No. 461-1-2) Wright Air Development Center, U. S. Air Force, Nov. 1952.

13. Larrabee, E. E.: Application of the Time-Vector Method to the Analysis of Flight Test Lateral Oscillation Data. FRM No. 189, Cornell Aero. Lab. Inc., Sept. 9, 1953.

14. Sternfield, L.: A Vector Method Approach to the Analysis of the Dynamic Lateral Stability of Aircraft. Jour. Aero. Sci., vol. 21, no. 4, Apr. 1954, pp. 251-256.

TABLE I

RANGES, DYNAMIC CHARACTERISTICS, AND SENSITIVITIES OF INSTRUMENTS

	Desirable characteristics of instruments for derivative investigation Free-oscillation maneuver			
Function	Range	Sensitivity, per inch deflection	Undamped natural frequency, cps	Damping ratio
α, deg	±10	5.0	8 or more	0.65
β, deg	±10	4.0	↓	↓
q, radian/sec	±0.2	0.2		
$\dot{q}$, radian/sec^2	±0.5	0.5		
r, radian/sec	±0.1	0.1		
$\dot{r}$, radian/sec^2	±0.4	0.4		
p, radian/sec	±0.2	0.2, rudder pulses		
	±0.6	0.6, aileron pulses		
$\dot{p}$, radian/sec^2	±0.6	0.6, rudder pulses		
	±6.0	6.0, aileron pulses		
a_n, g units	±1	1.0		
a_t, g units	±0.3	0.3, rudder pulses		
	±0.6	0.6, aileron pulses		

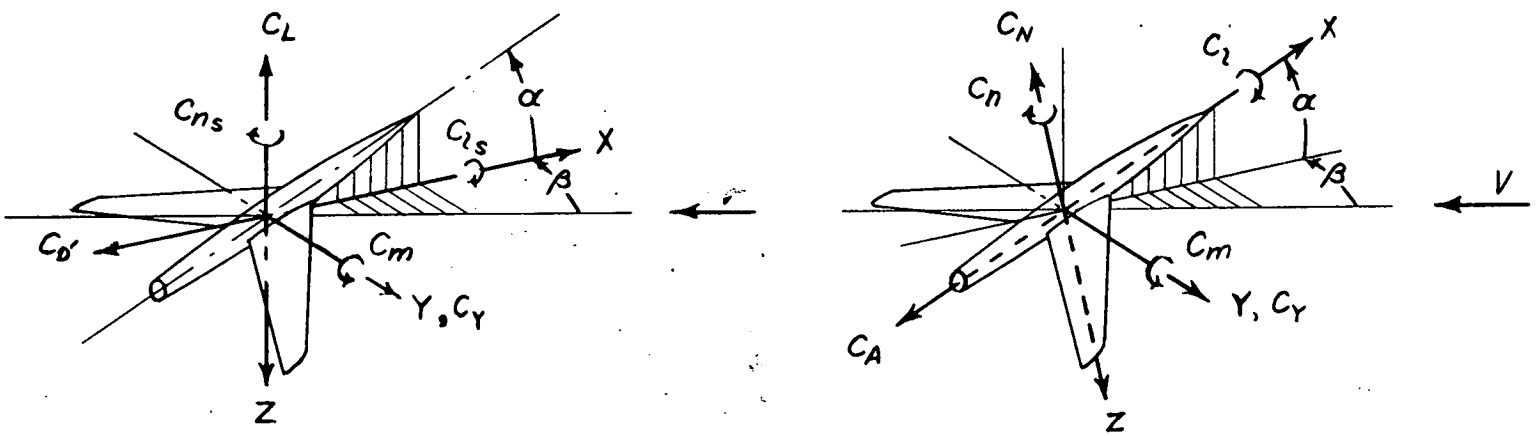

Stability axes

Body axes

Figure 1.- Systems of axes. (Positive values of direction, force, moments, and angles are indicated by arrows.)

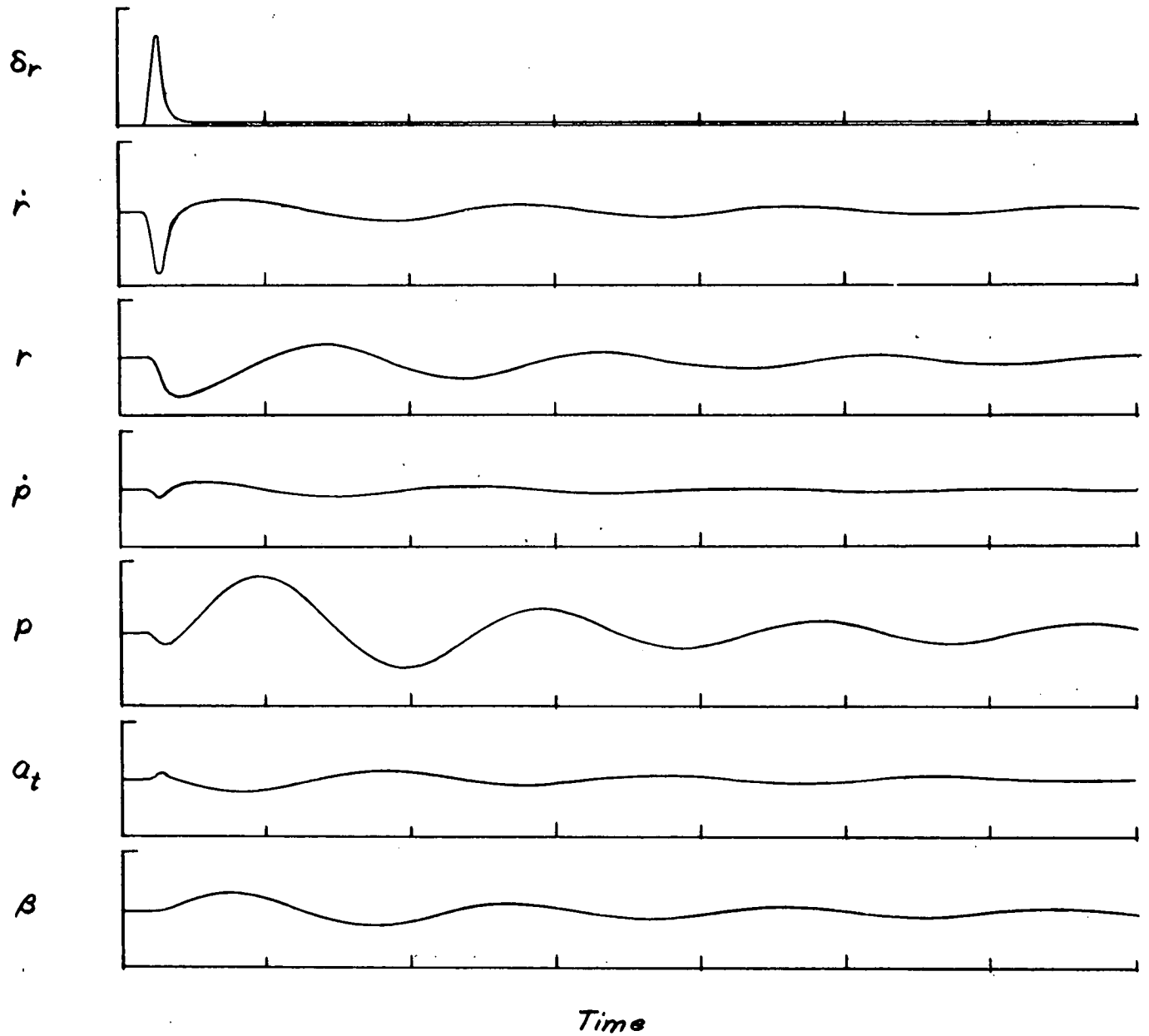

Figure 2.- Time history of a well performed free-oscillation maneuver.

Trace	Instrument		Scale factors	
	Nat. freq	Damp. ratio	Flt's. 20→	Flt's.
p	6.75	0.65	0.511	
r	6.75	.65	.126	
a_t	19.50	.65	.490	
β	10.50	.65	10.30	

β-vane location

$X_v =$ _____ ; $Z_v =$ _____

Linear accelerometer location

$X =$ _____ ; $Y =$ _____ ; $Z =$ _____

$S =$ _____

1	2	3	4	5	6	7	8	9	10
Comment	Flt.-Run	h_p, ft	M	V, fps	Dynamic pressure, $\bar{q}$	Weight, W, lb	C.G., % MAC	$C_{L_t} = \frac{W}{\bar{q}S}$	Density, ρ, slugs/ft^3
	20-17	40,320	0.745	723	142	23,800	28.7	0.237	.000573

Trace	Instrument		Scale factors	
	Nat. freq	Damp. ratio	Flt's. 20→	Flt's.
α	10.5	.65	10.6	
a_n	32.0	.65	5.17	
δ_r			13.4	
δ_a			16.7	

Airplane _____

Configuration _____

_____

11	12	13	14	15	16	17	18	19
α, deg / a_n, trim, g units	δ_e, trim, deg	Control input, $\Delta\delta$, deg	Period, P, sec	$T_{1/2}$, sec	$\omega_{n_d} = \frac{2\pi}{P}$	Damping angle $\Phi_d = \tan^{-1}\left(\frac{1.103P}{T_{1/2}}\right)$	Damping ratio $\zeta = \sin\Phi_d$	Undamped nat. freq. $\omega_n = \omega_{n_d}/\cos\Phi_d$
6.5 / .93		-7.55	3.66	2.92	1.72	7.56	0.131	1.73

Figure 3.- Format of table used by NASA HSFS to record actual conditions at time of maneuver.

$$K_t = 2Ka^2$$

$$K_t > Wz_a + Wz_c \quad \text{(for stability of the experimental installation)}$$

$$z_a = \frac{K_{t_2} - K_{t_1}\left(\frac{P_1}{P_2}\right)^2}{W\left[1 - \left(\frac{P_1}{P_2}\right)^2\right]} - \frac{W_c z_c}{W}$$

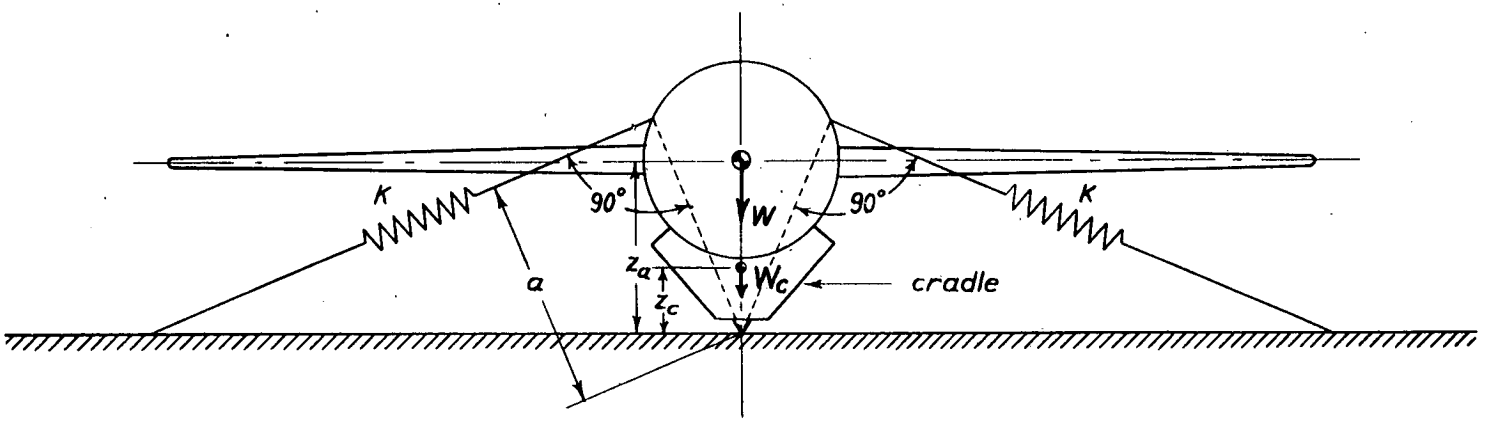

Figure 4.- Determination of rolling moment of inertia.

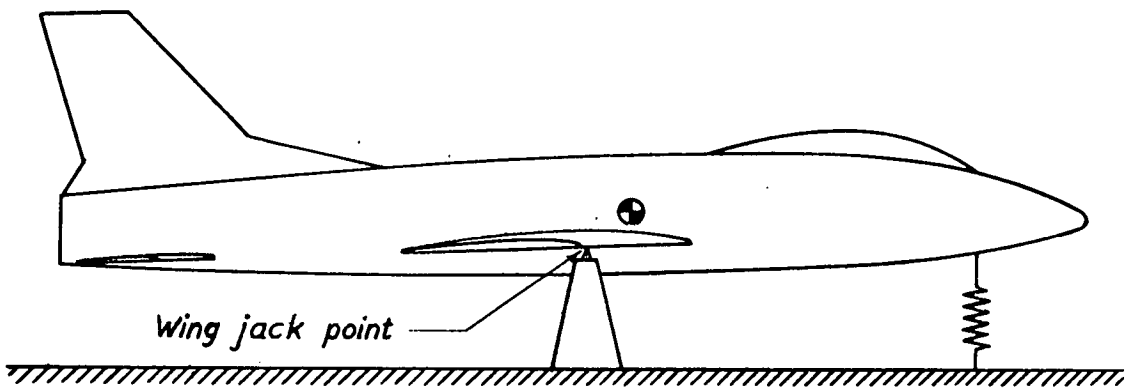

Figure 5.- Determination of pitching moment of inertia.

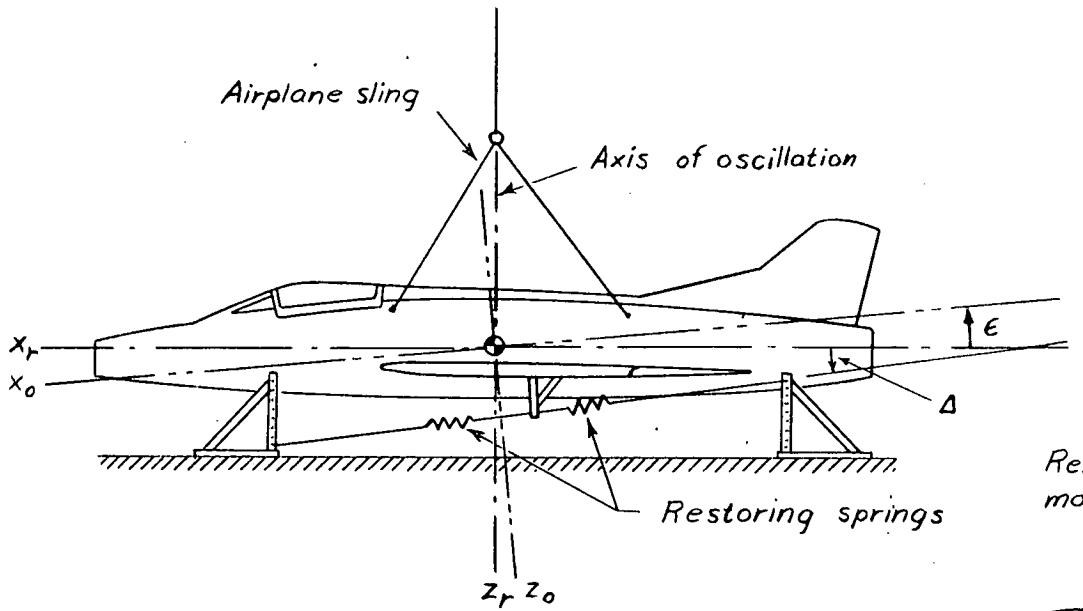

(a) Test setup.

$$\tan \epsilon = \frac{zI_{z_r}}{I_{z_r} - I_{x_r}} \tan \Delta$$

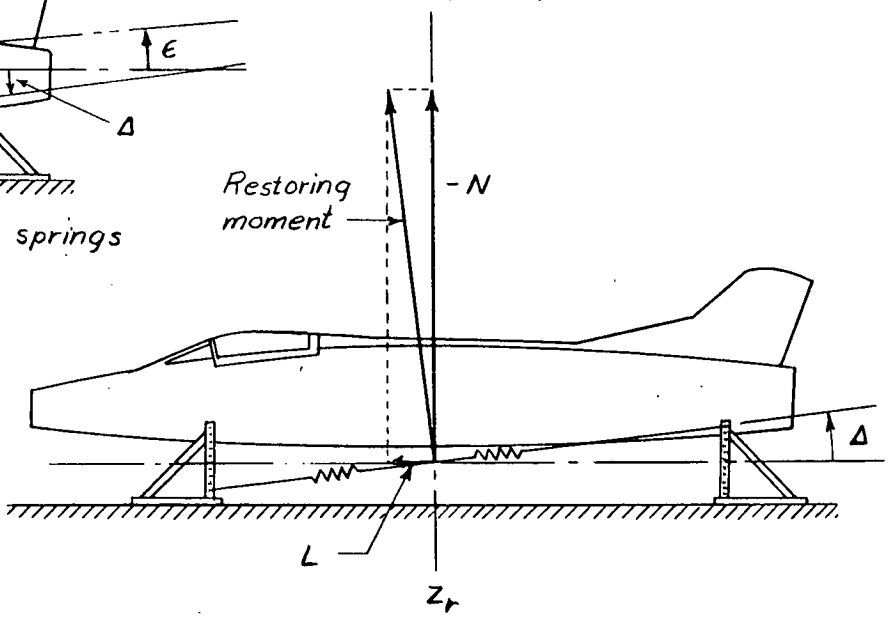

(b) Vector resolution.

Figure 6.- Determination of inclination of principal axis and yawing moment of inertia.

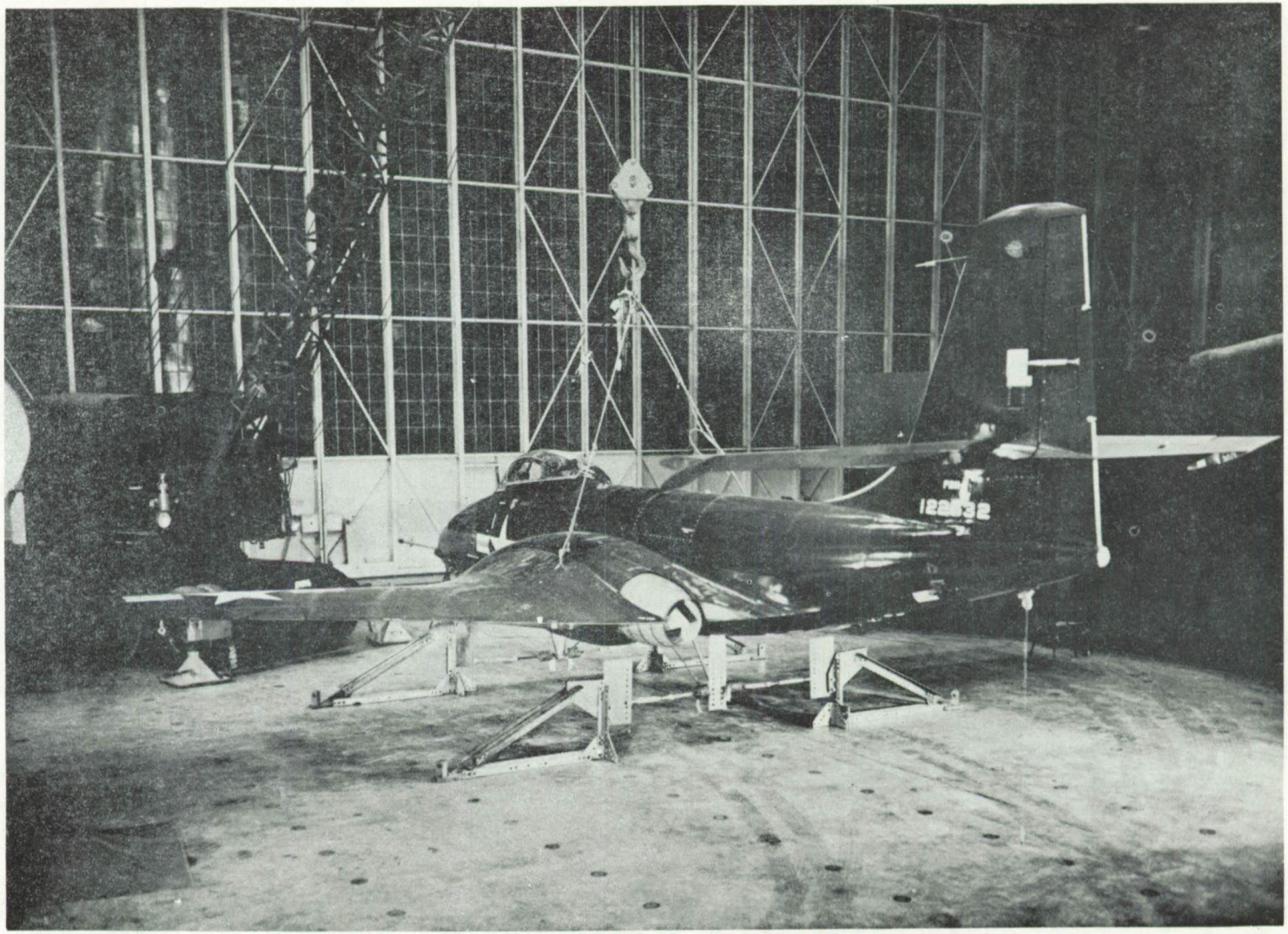

Figure 8.- Photograph showing a general arrangement for determining inclination of principal axis. Springs attached to mounting brackets below fuselage.

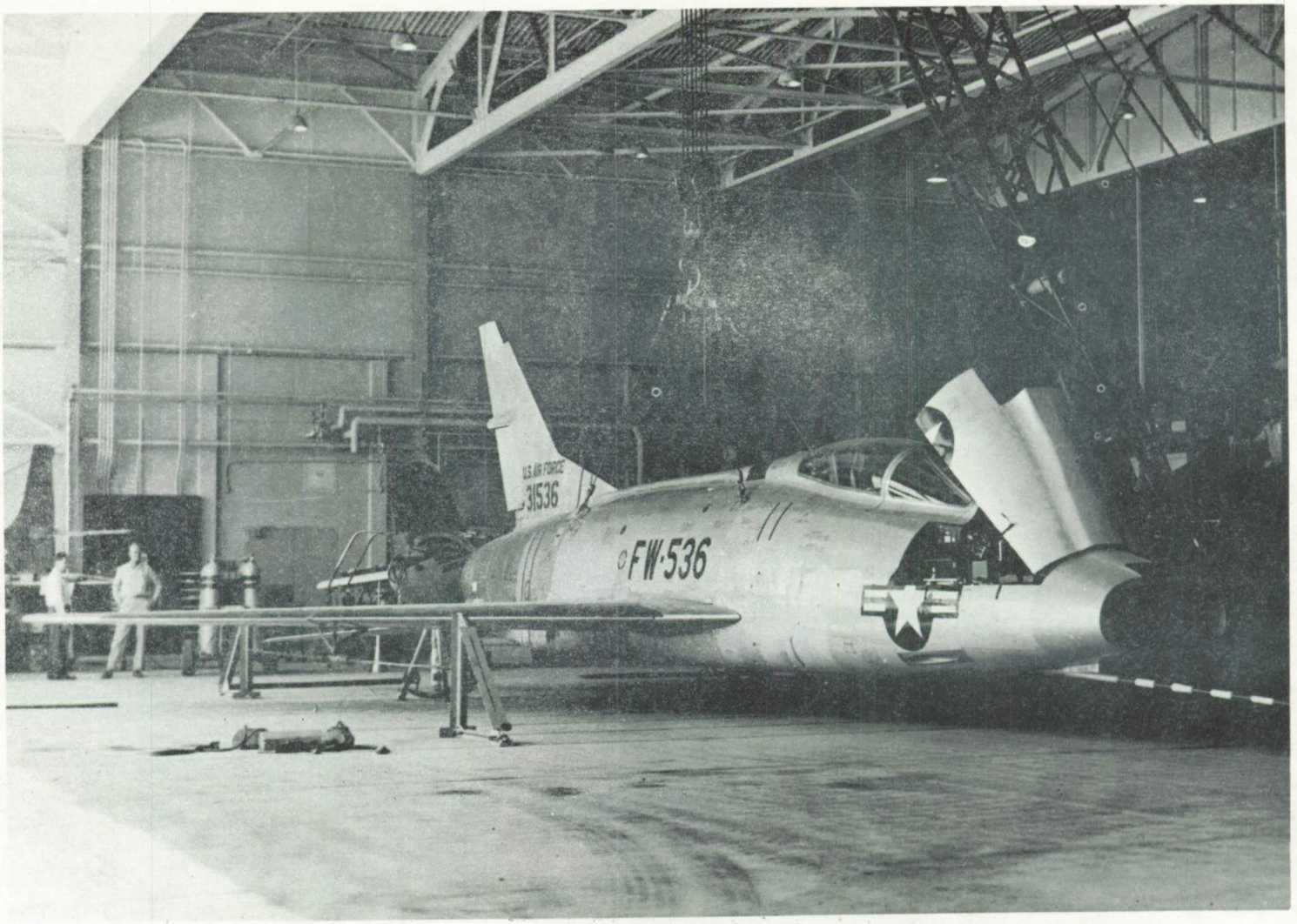

Figure 7.- Photograph showing a general arrangement for determining inclination of principal axis and yawing moment of inertia. Springs attached to mounting brackets located below wings.

Instrument	Mounting error
p_i	ψ_1 θ_1 ϕ_1
q_i	ψ_2 θ_2 ϕ_2
r_i	ψ_3 θ_3 ϕ_3

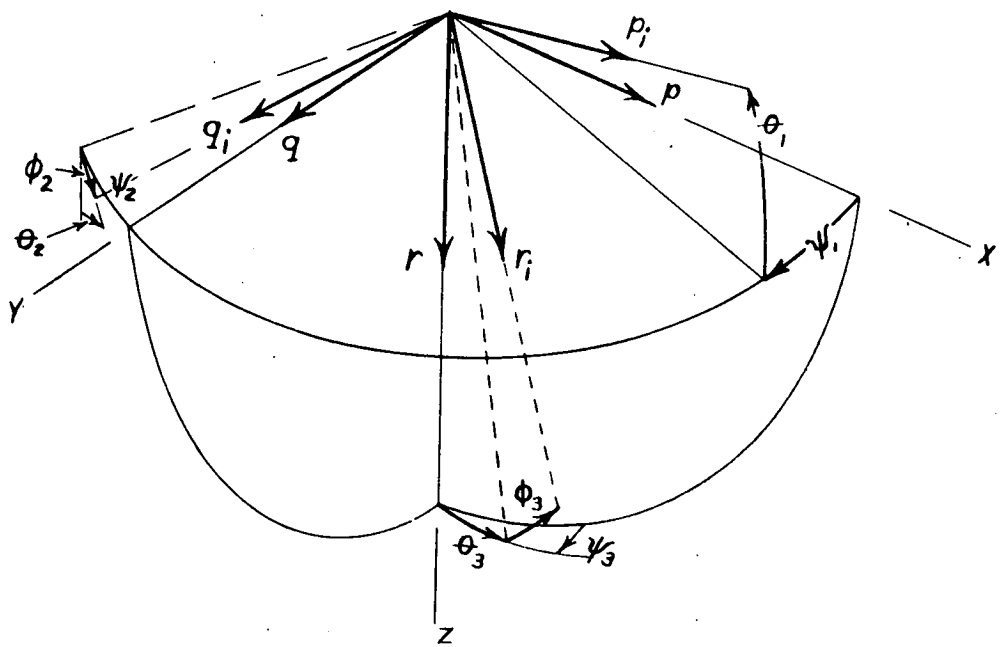

$$p_i = p \cos\theta_1 \cos\psi_1 + q \cos\theta_1 \sin\psi_1 - r \sin\theta_1$$

$$q_i = p (\cos\psi_2 \sin\theta_2 \sin\phi_2 - \sin\psi_2 \cos\phi_2) + q (\sin\psi_2 \sin\theta_2 \sin\phi_2 + \cos\psi_2 \cos\phi_2) + r (\cos\theta_2 \sin\phi_2)$$

$$r_i = p (\cos\psi_3 \sin\theta_3 \cos\phi_3 + \sin\psi_3 \sin\phi_3) + q (\sin\psi_3 \sin\theta_3 \cos\phi_3 - \cos\psi_3 \sin\phi_3) + r (\cos\theta_3 \cos\phi_3)$$

Note: Solve for p, q, and r

Figure 9.- Equations for correcting rate gyro records for instrument misalinement.

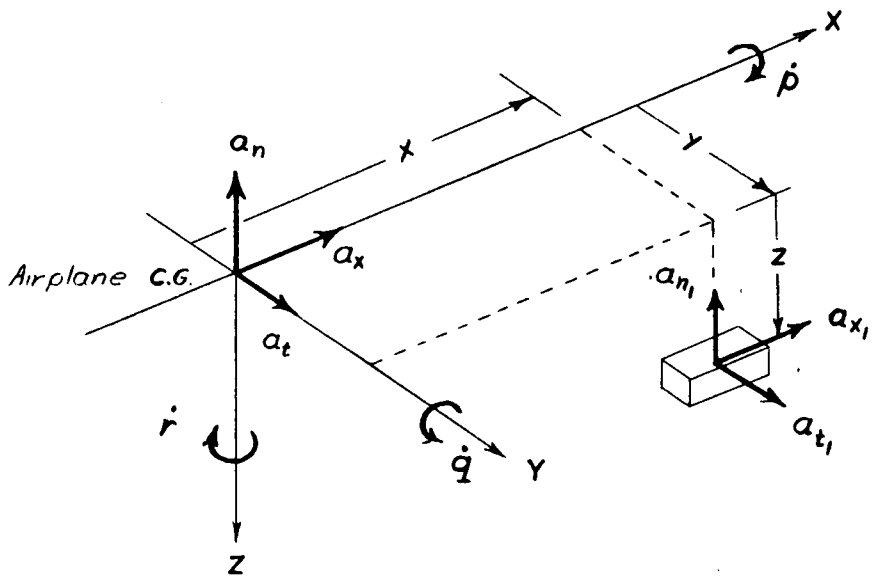

$$a_x = a_{x_1} - \frac{z\dot{q}}{g} + \frac{y\dot{r}}{g} + \frac{xq^2}{g} + \frac{xr^2}{g}$$

$$a_t = a_{t_1} - \frac{x\dot{r}}{g} + \frac{z\dot{p}}{g} + \frac{yr^2}{g} + \frac{yp^2}{g}$$

$$a_n = a_{n_1} - \frac{x\dot{q}}{g} + \frac{y\dot{p}}{g} - \frac{zq^2}{g} - \frac{zp^2}{g}$$

Figure 10 .- Equations for correcting records of linear accelerometers to the center of gravity of the aircraft.

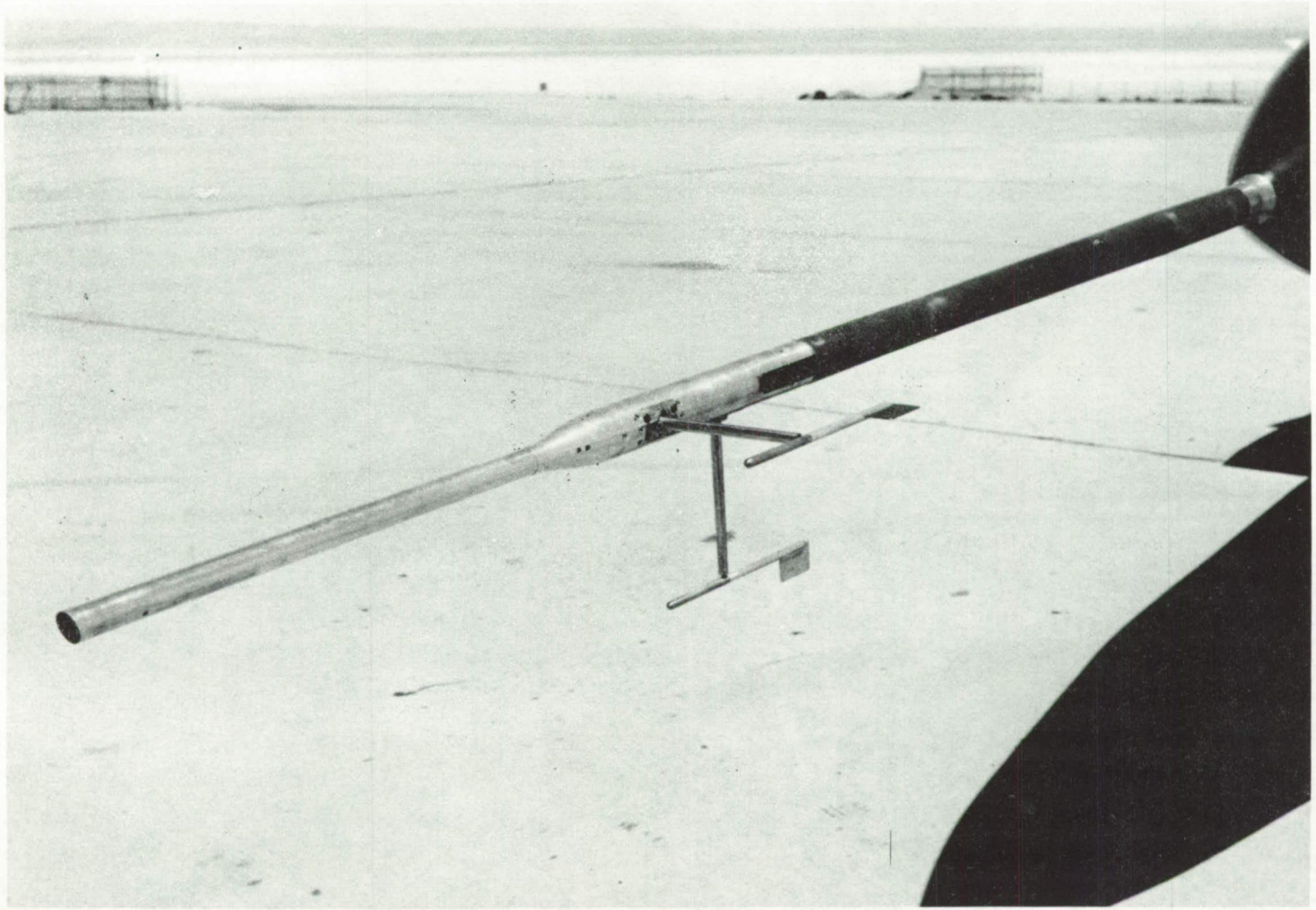

Figure 11.- Photograph of a typical NASA installation of angle-of-attack and sideslip vanes on nose boom.

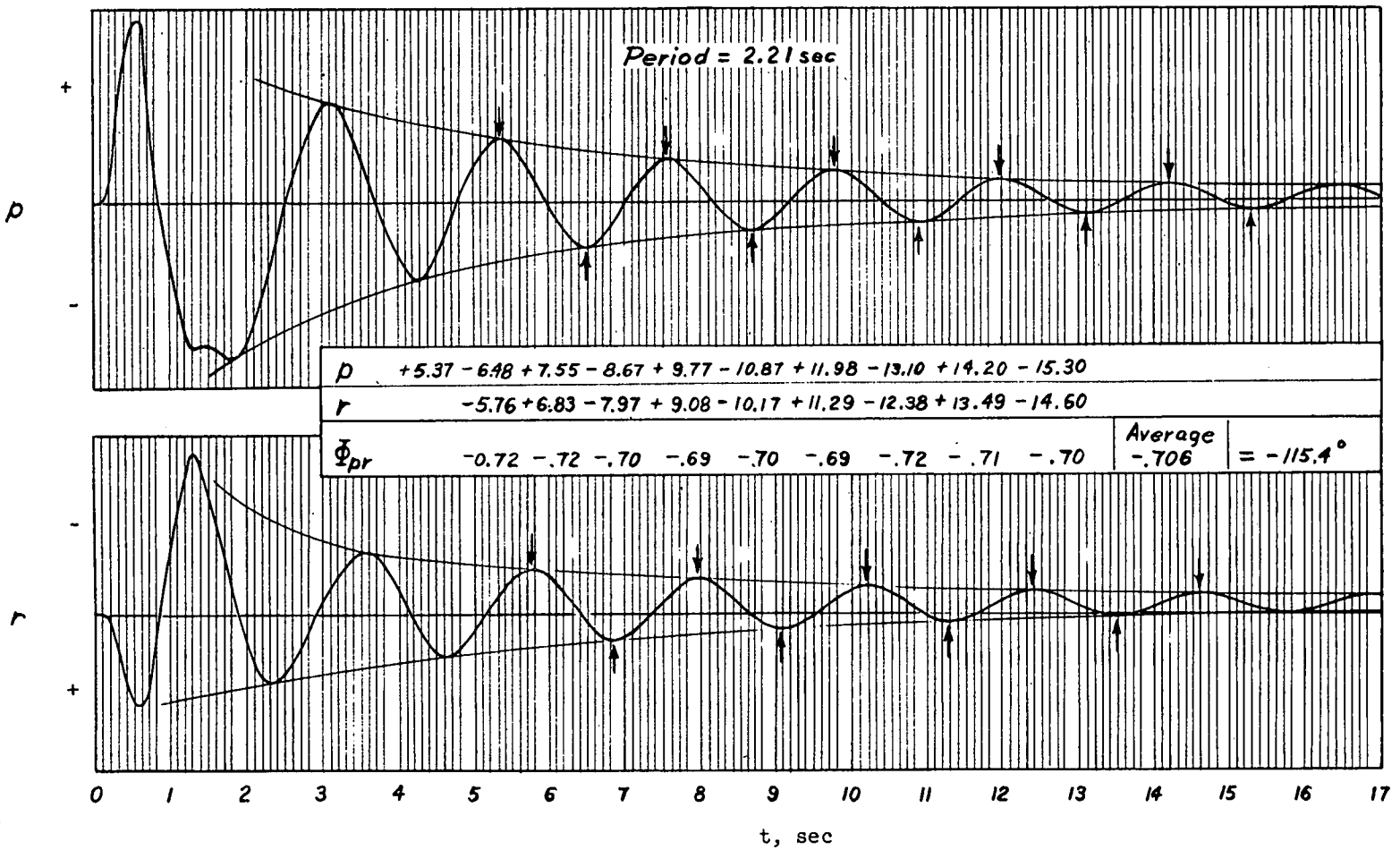

(a) Period and phase angles.

Figure 12.- Determination of period, time-to-damp to one-half amplitude, and the phase angles and amplitude ratios from free-oscillation data.

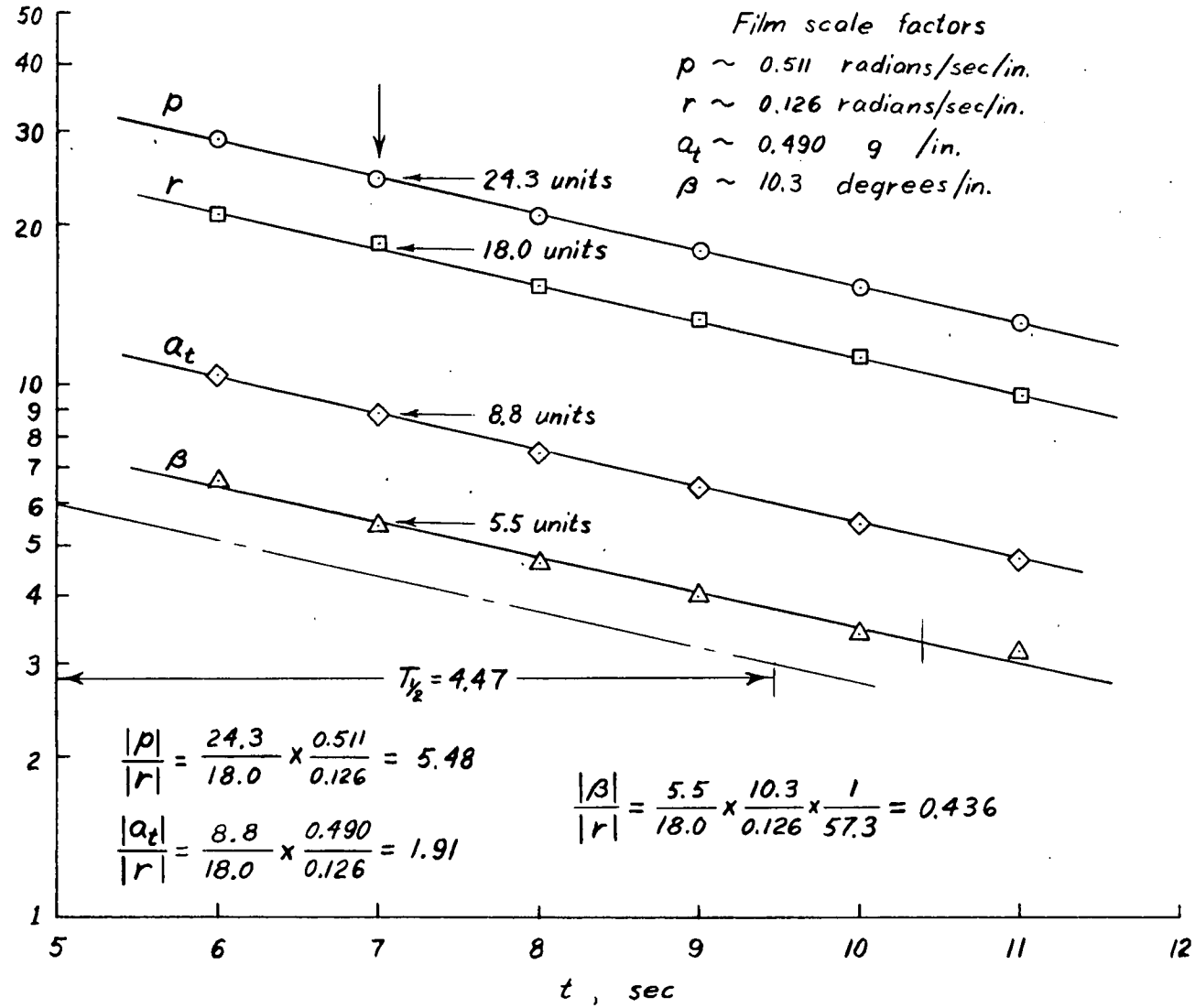

(b) $T_{1/2}$ and amplitude ratios.

Figure 12.- Concluded.

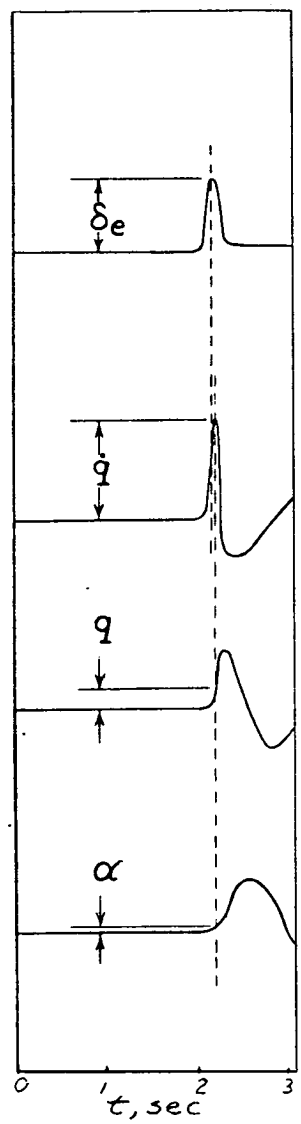

Figure 13.- Typical determination of flight quantities for the evaluation of longitudinal control derivatives.

$$\frac{|a_n|}{|q|} e^{i\Phi_{a_n q}} = \frac{|a_{n_i}|}{|q|} e^{i\Phi_{a_{n_i} q}} + \frac{x}{g}\frac{|\dot{q}|}{|q|} e^{i\Phi_{\dot{q}q}}$$

$$\frac{|a_n|}{|q|} e^{i\Phi_{a_n q}} + \frac{V}{g}\frac{|q|}{|q|} e^{i\Phi_{qq}} - \frac{V}{g}\frac{|\dot{\alpha}|}{|q|} e^{i\Phi_{\dot{\alpha}q}} = 0$$

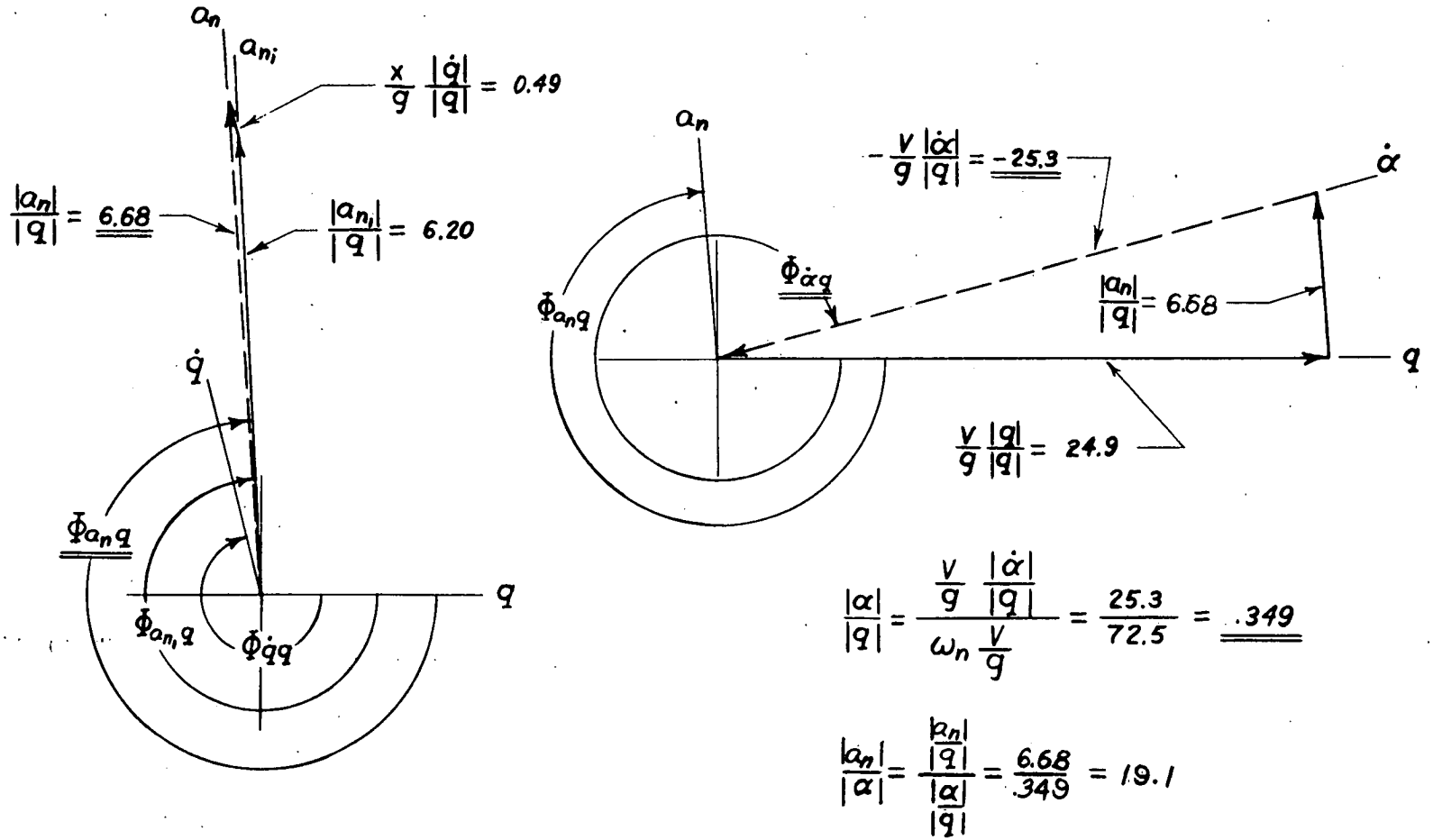

$$\frac{|\alpha|}{|q|} = \frac{\frac{V}{g}\frac{|\dot{\alpha}|}{|q|}}{\omega_n \frac{V}{g}} = \frac{25.3}{72.5} = .349$$

$$\frac{|a_n|}{|\alpha|} = \frac{\frac{|a_n|}{|q|}}{\frac{|\alpha|}{|q|}} = \frac{6.68}{.349} = 19.1$$

Figure 14.- Vector solution of $\frac{|a_n|}{|\alpha|}$ using pitch rate as base for amplitude ratios when angle-of-attack records are available.

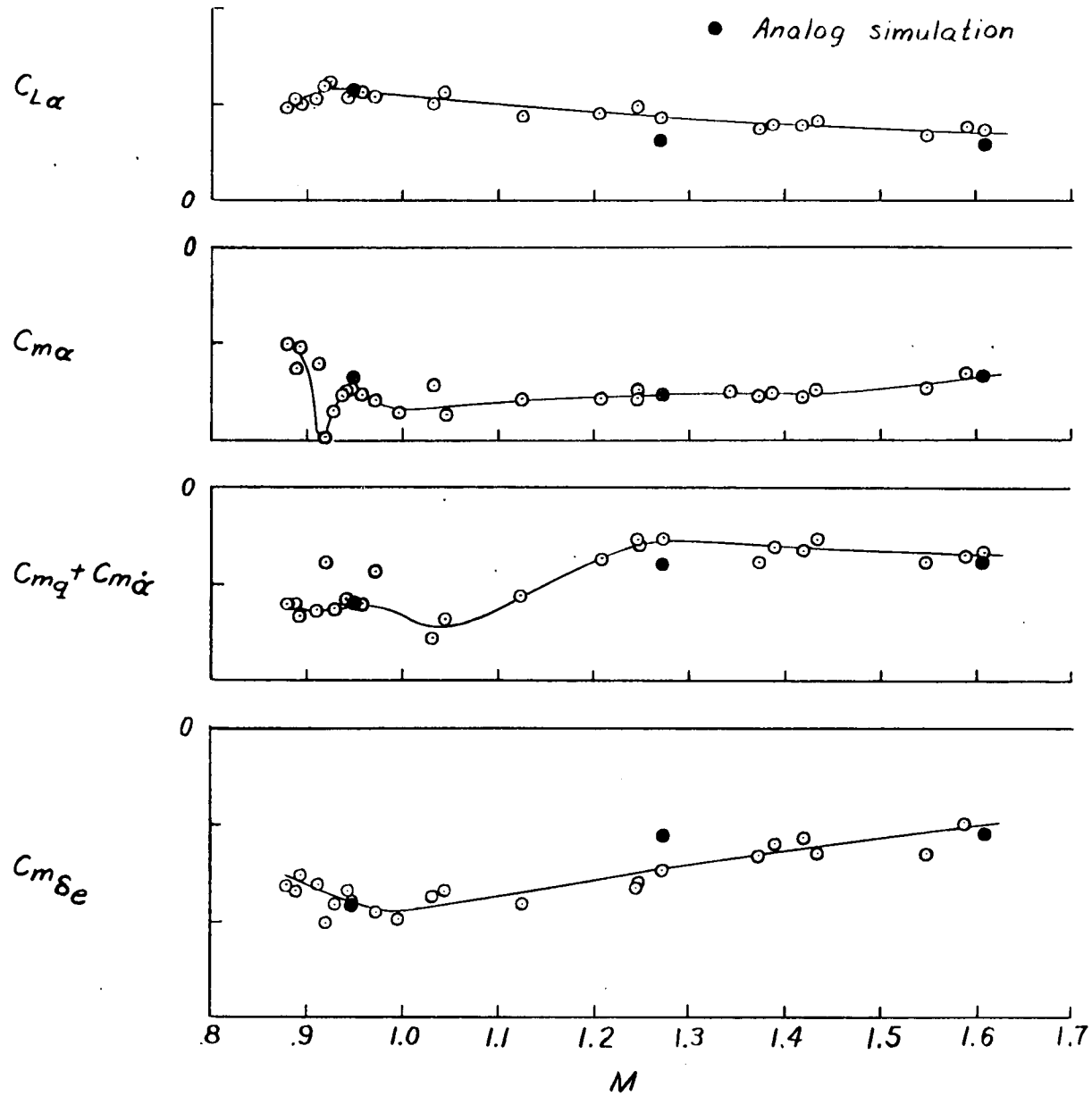

Figure 15.- Typical results of an analysis for the longitudinal stability and control derivatives.

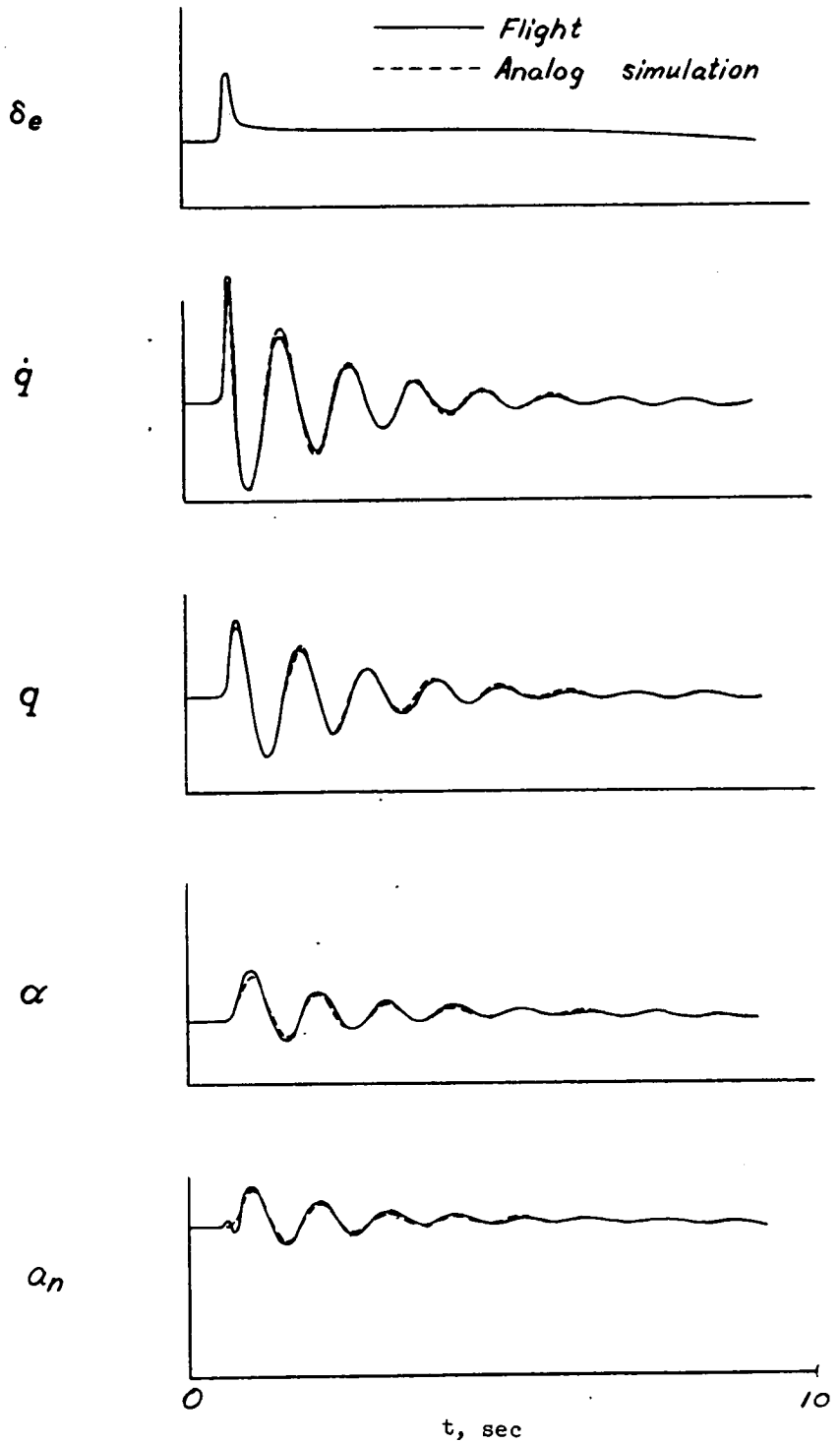

Figure 16.- Comparison of analog-simulated time history of a longitudinal maneuver with flight time history.

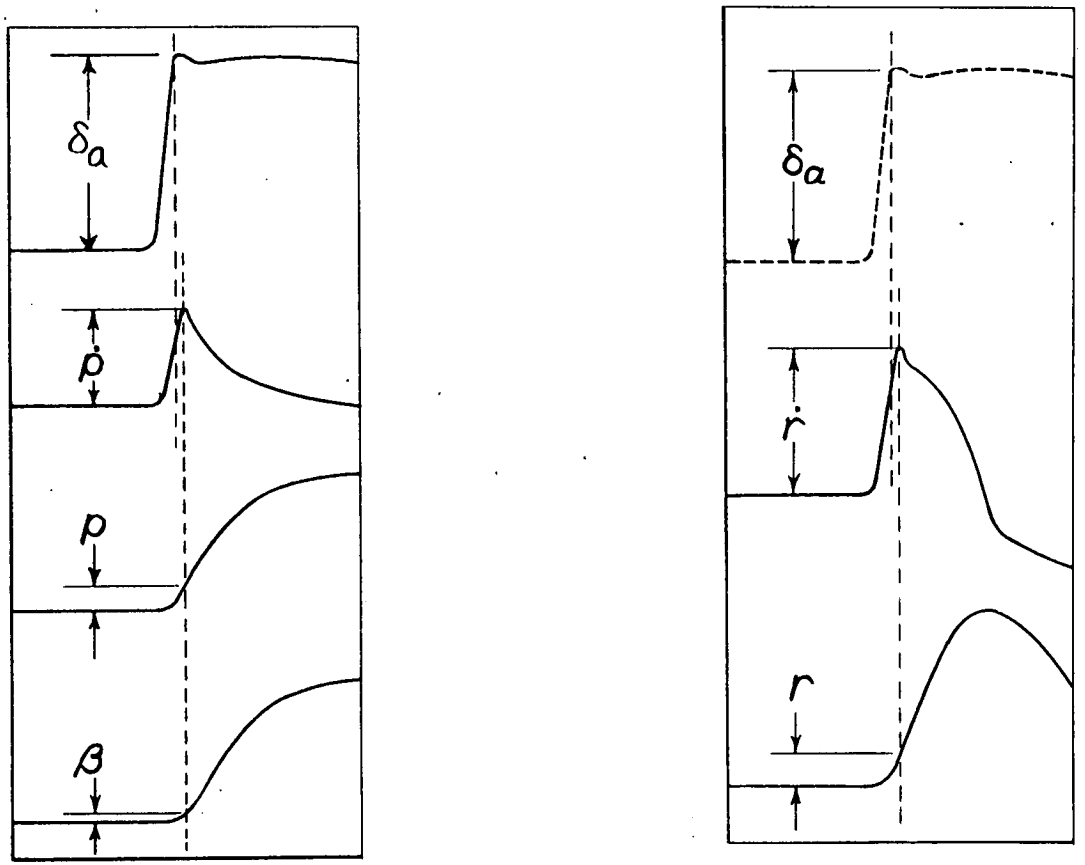

Figure 17.- Typical determination of flight quantities for the evaluation of lateral control derivatives.

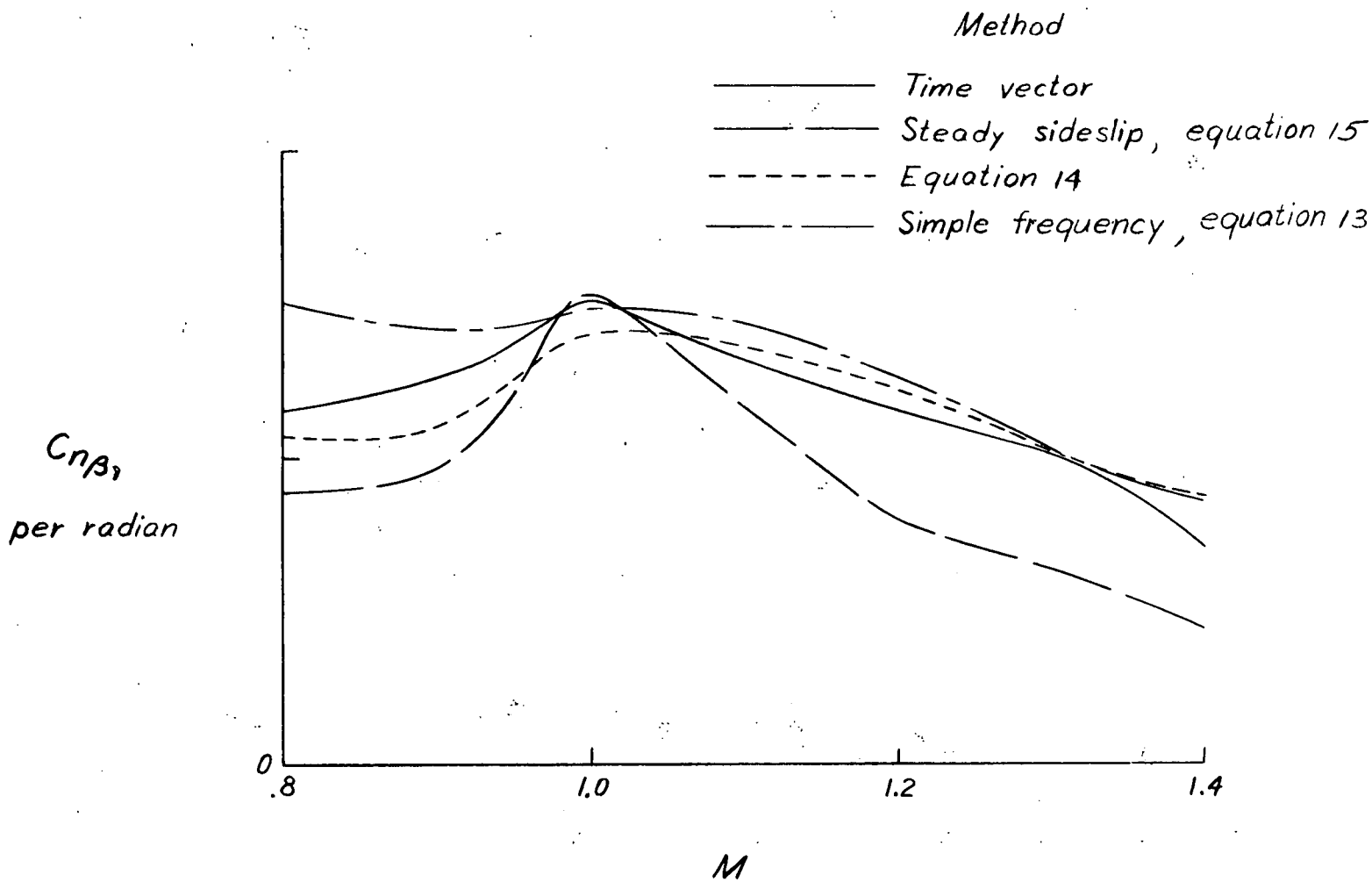

Figure 18.- Comparison of C_{n_β} as determined by several different approximate methods with the time-vector method.

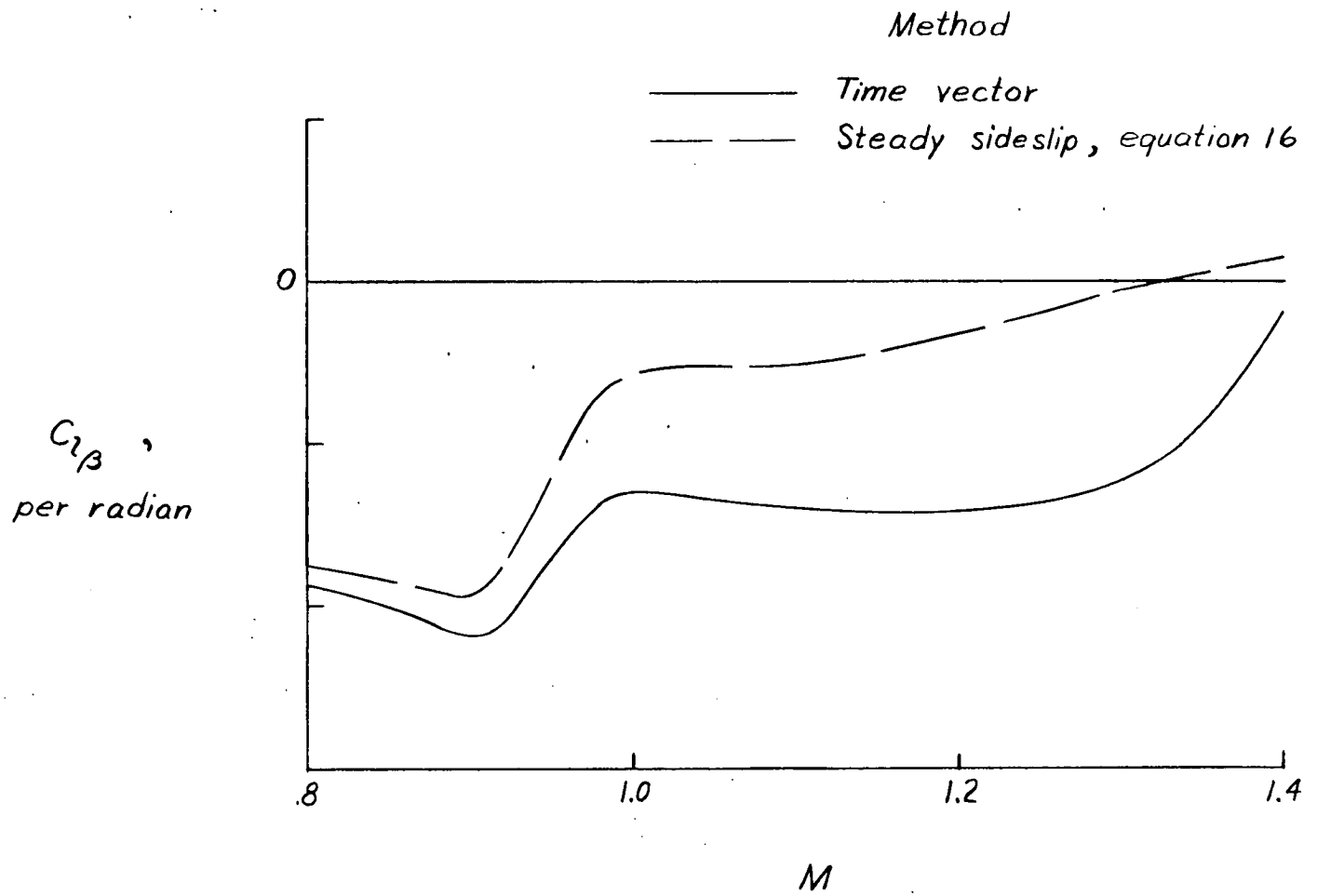

Figure 19.- Comparison of results of determining C_{l_β} by time-vector method and steady-sideslip equations.

$$\frac{|a_t|}{|r|}e^{i\Phi_{a_t r}} = \frac{|a_{t_1}|}{|r|}e^{i\Phi_{a_{t_1} r}} - \frac{x}{g}\frac{|\dot{r}|}{|r|}e^{i\Phi_{\dot{r}r}} + \frac{z}{g}\frac{|\dot{p}|}{|r|}e^{i\Phi_{\dot{p}r}}$$

$$2\mathcal{I}\frac{|\dot{\beta}|}{|r|}e^{i\Phi_{\dot{\beta}r}} + 2\mathcal{I}\frac{|r|}{|r|}e^{i\Phi_{rr}} - 2\mathcal{I}\alpha\frac{|p|}{|r|}e^{i\Phi_{pr}} - C_{L_t}\frac{|\phi|}{|r|}e^{i\Phi_{\phi r}} - C_{L_t}\frac{|a_t|}{|r|}e^{i\Phi_{a_t r}} = 0$$

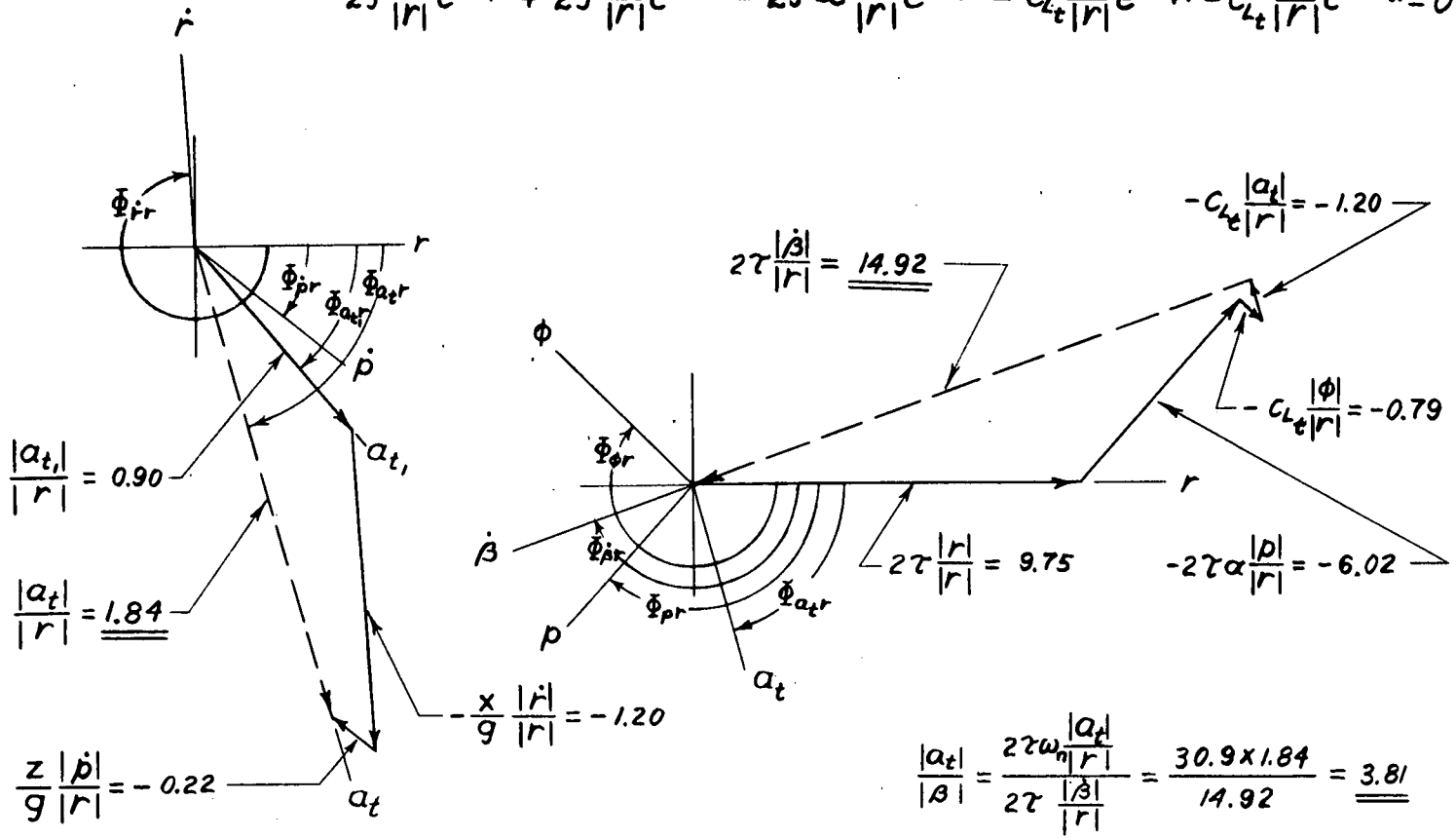

Figure 20.- Vector solution of $\frac{|a_t|}{|\beta|}$ using yaw rate as base for amplitude ratios when sideslip records are unavailable.

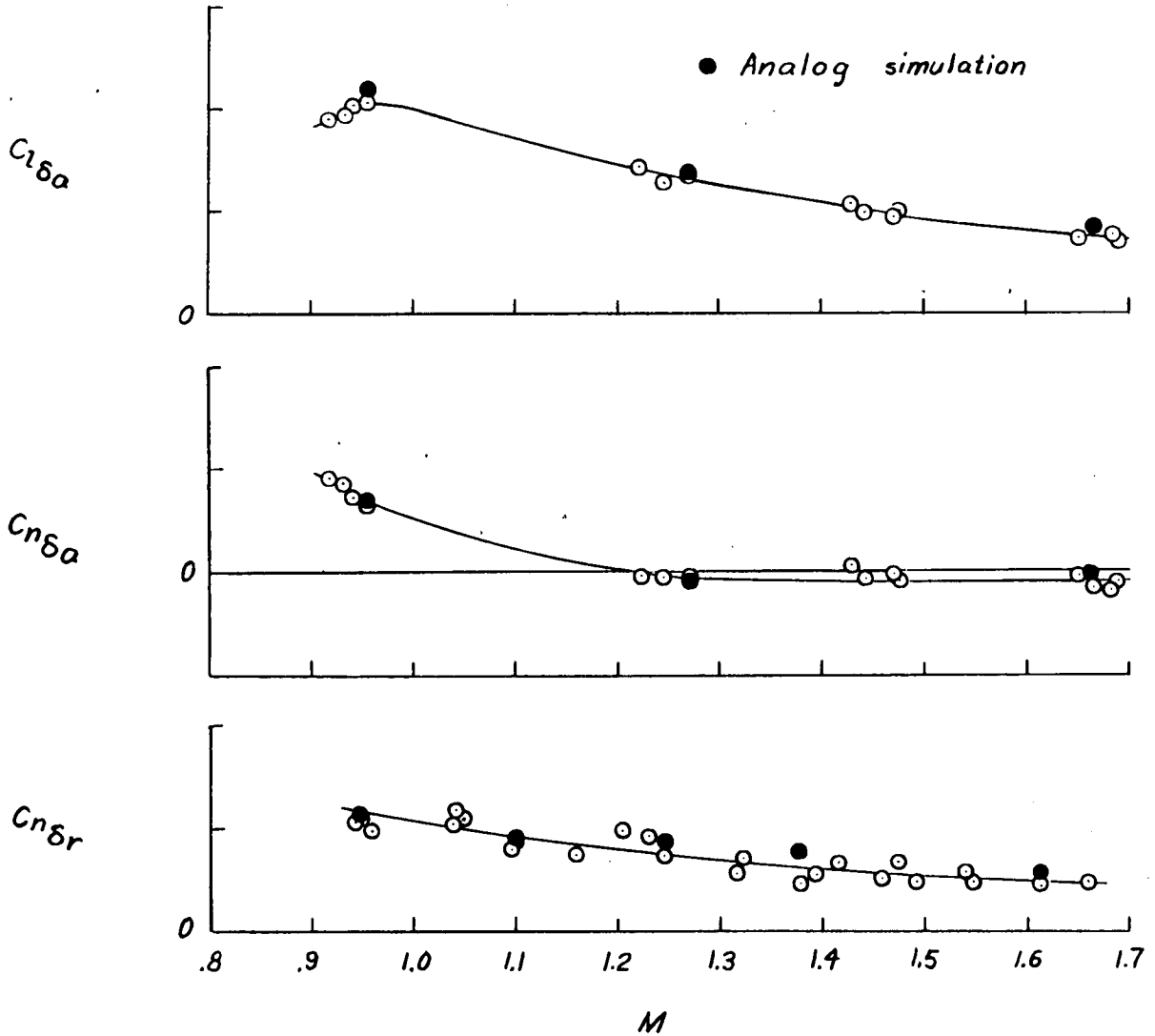

(a) Control derivatives.

Figure 21.- Typical results of an analysis for the lateral stability and control derivatives.

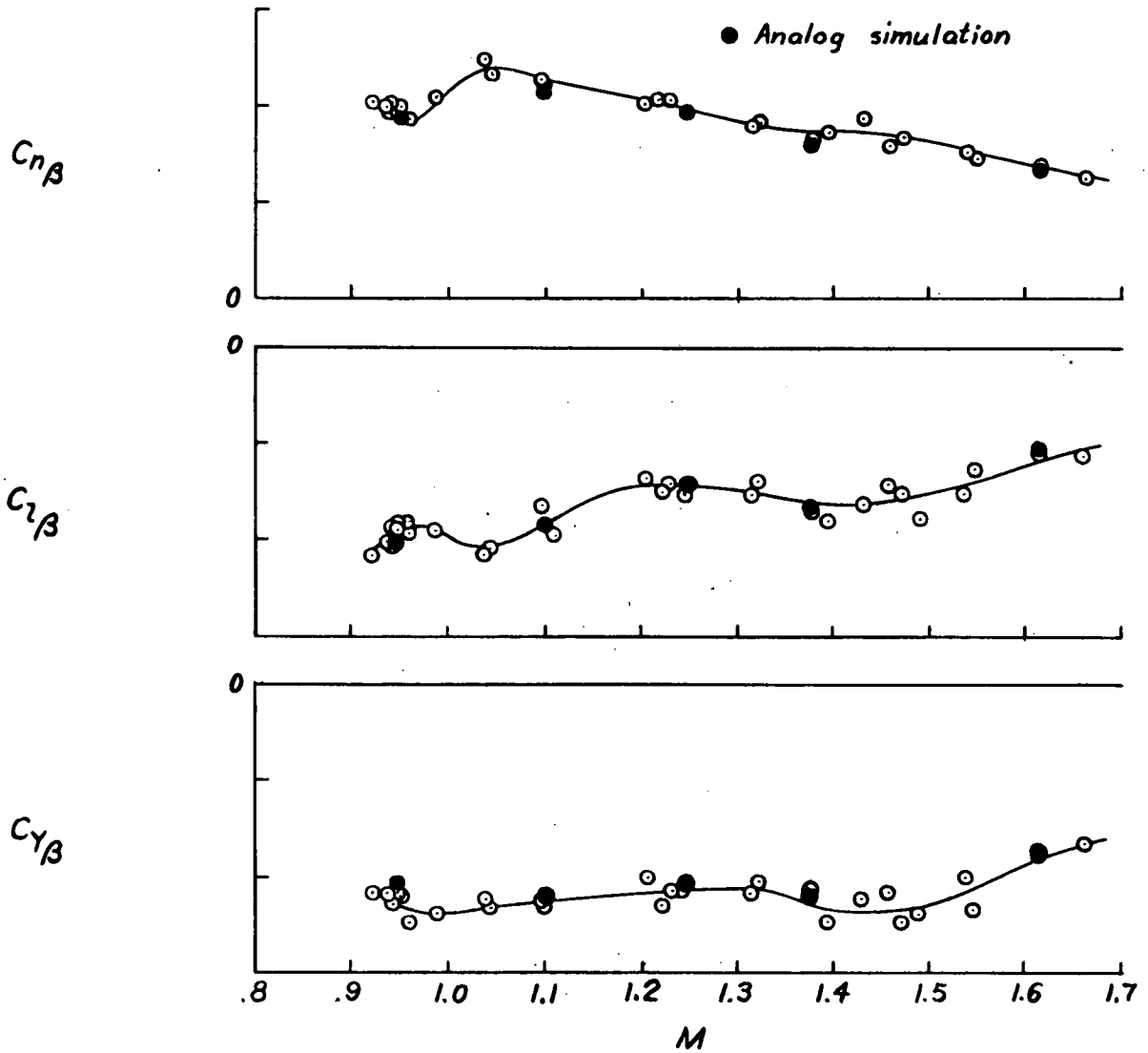

(b) Static derivatives.

Figure 21.- Continued.

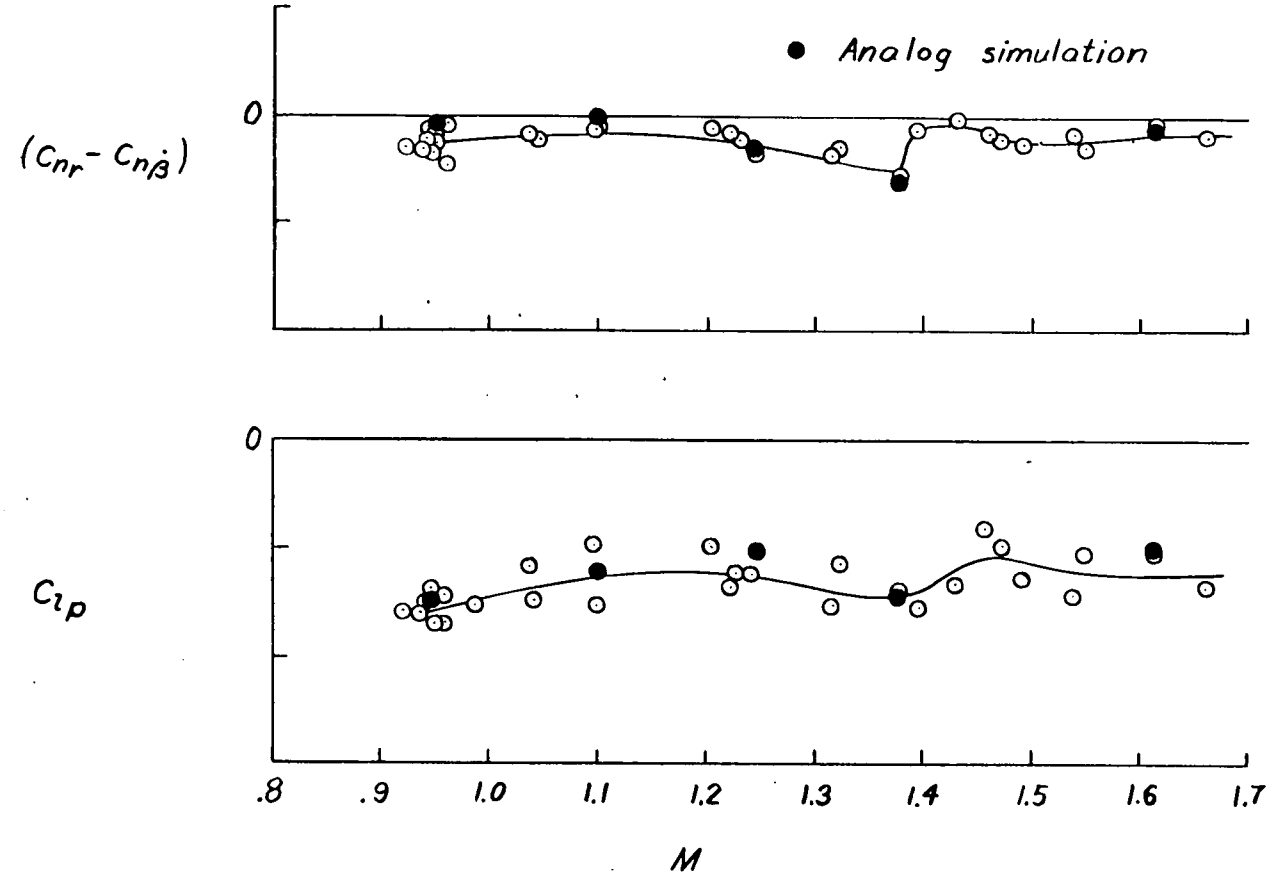

(c) Damping derivatives.

Figure 21.- Concluded.

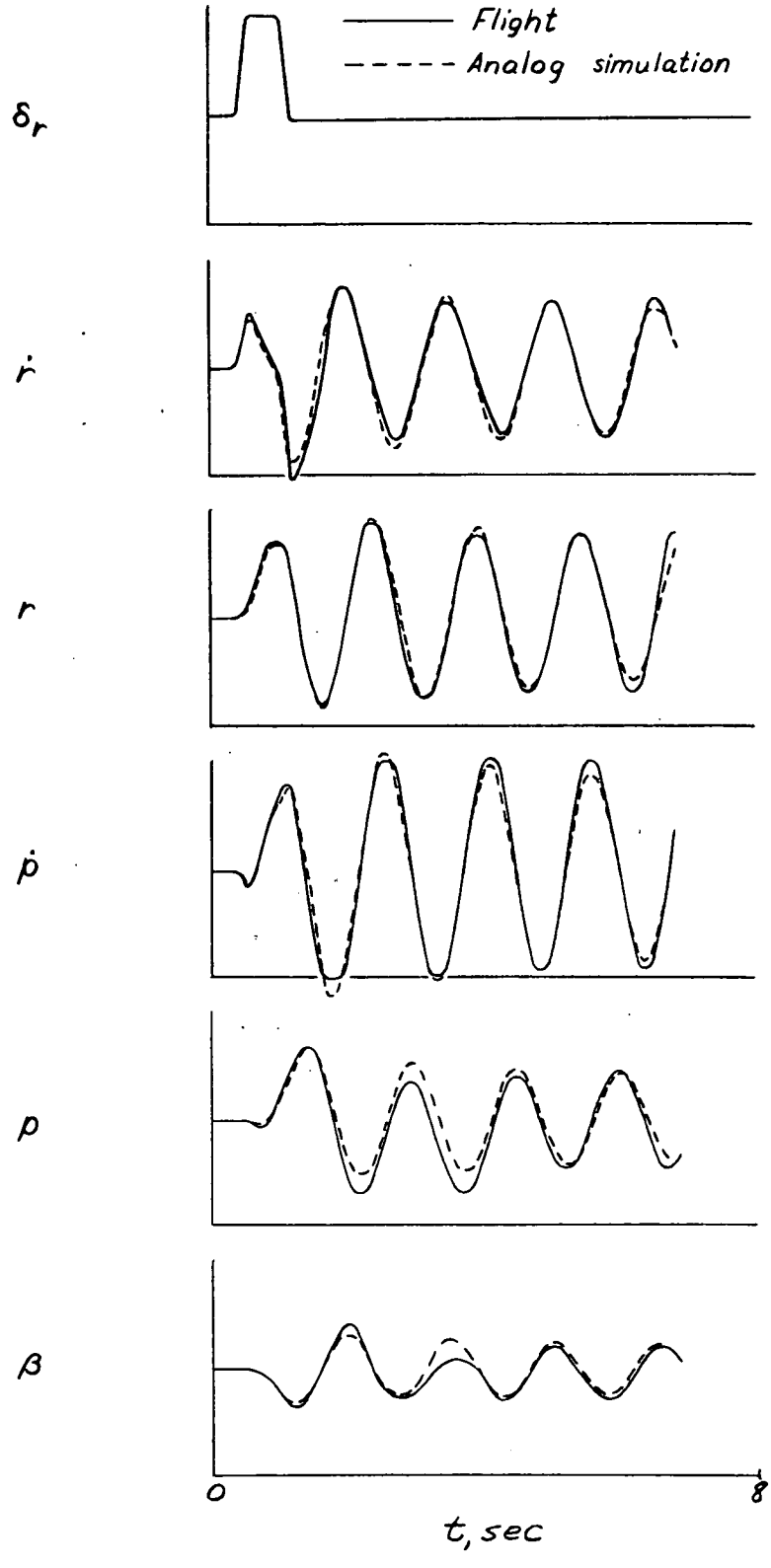

Figure 22 .- Comparison of analog-simulated time history of a lateral maneuver with flight time history.

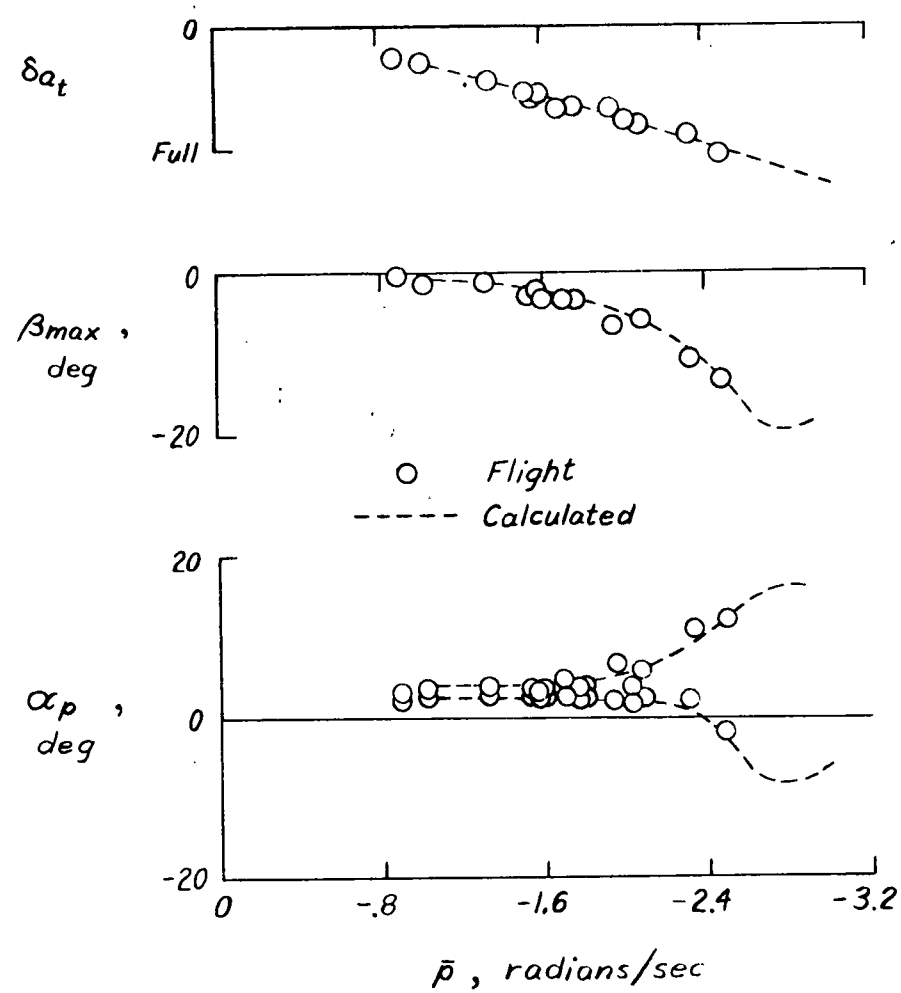

Figure 23.- Comparison with flight data of results of analog simulation studies of 360° rolls using flight-determined derivatives.

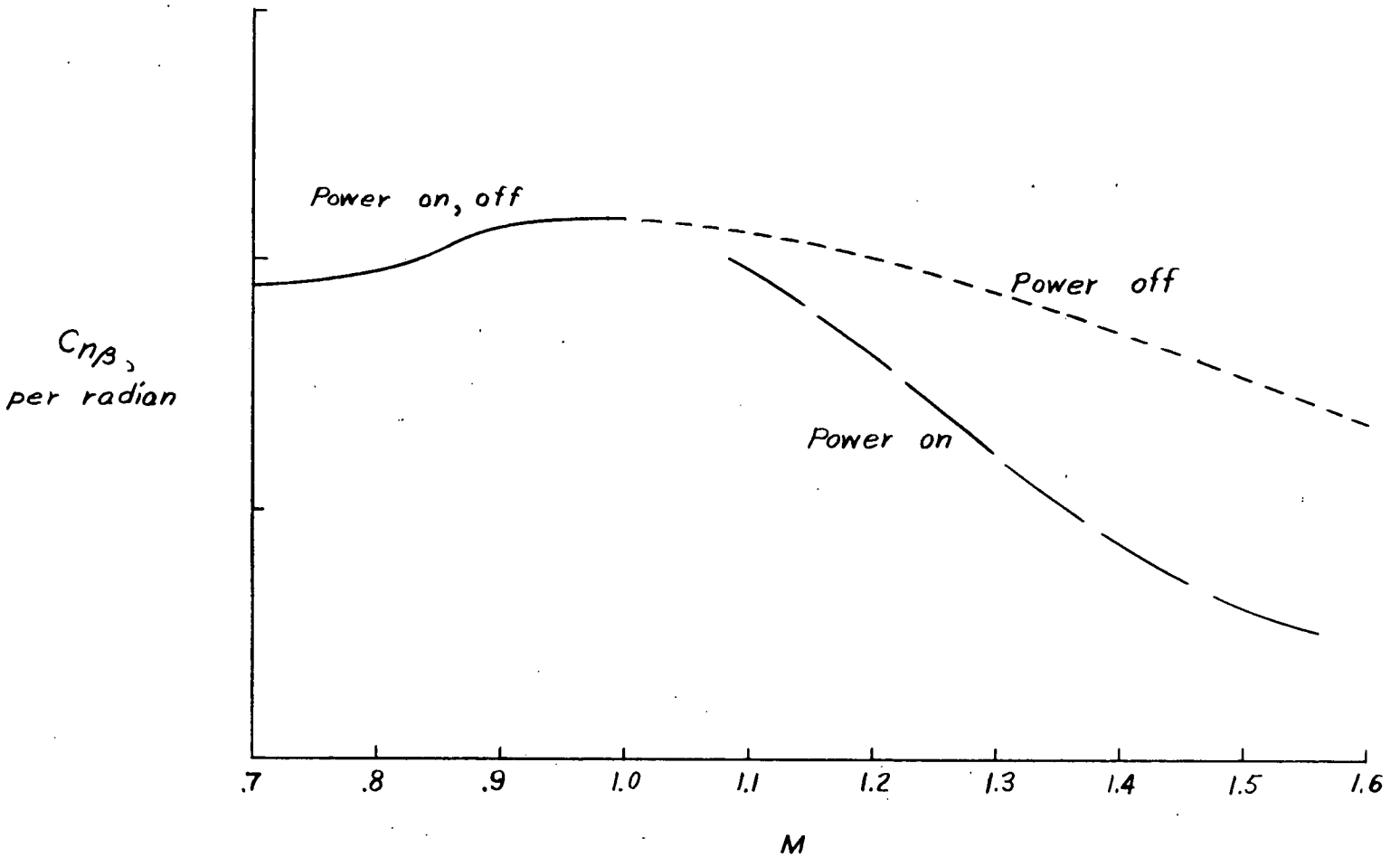

Figure 24.- Influence of jet exhaust of a rocket engine on the directional stability derivative C_{n_β}.

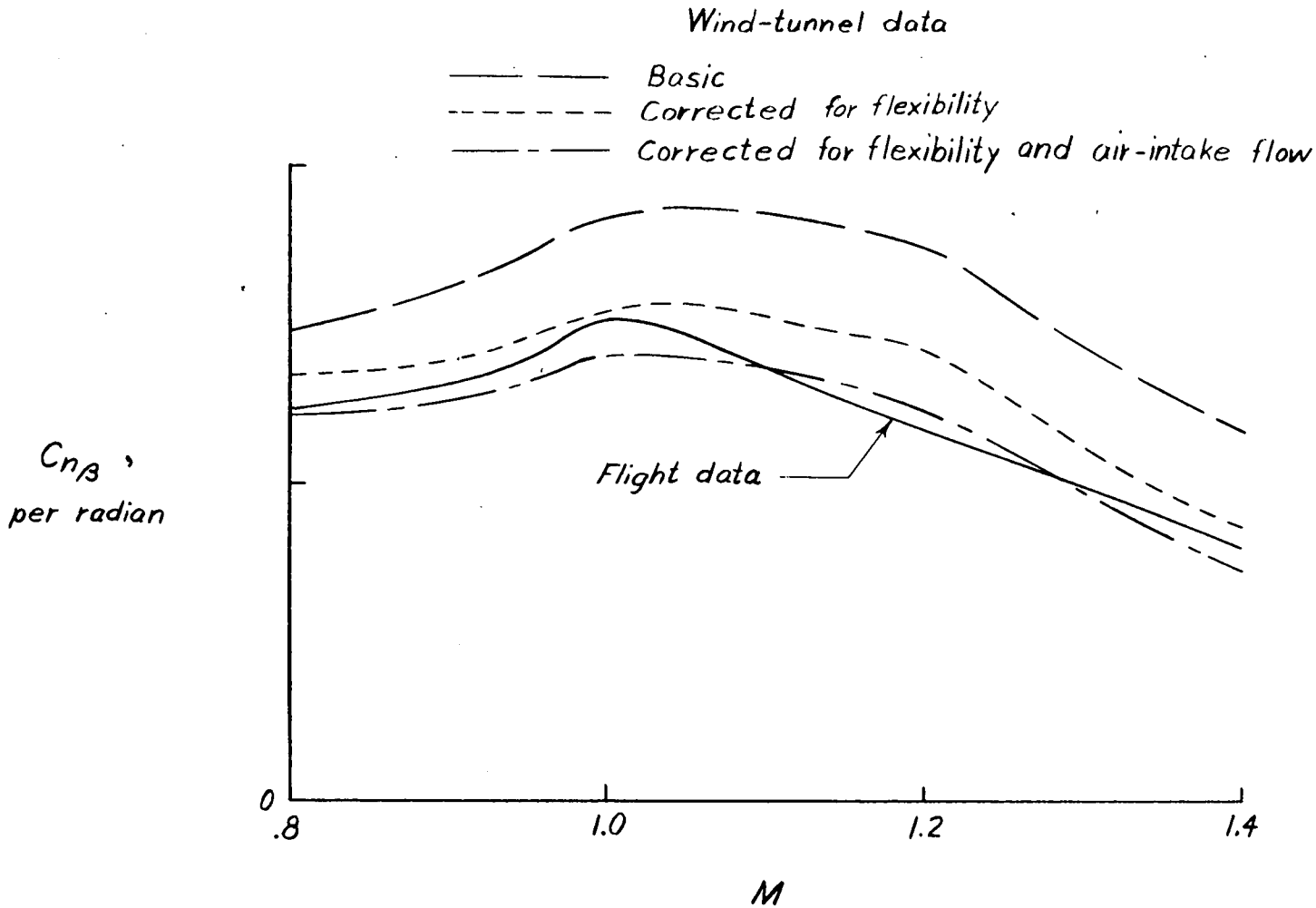

Figure 25.- Influence of flexibility and air intake to engine on the directional stability derivative C_{n_β}.

$$2\tau\frac{|\dot{\beta}|}{|r|}e^{i\Phi_{\dot{\beta}r}} + 2\tau\frac{|r|}{|r|}e^{i\Phi_{rr}} - 2\tau\alpha\frac{|p|}{|r|}e^{i\Phi_{pr}} - C_{L_t}\frac{|\phi|}{|r|}e^{i\Phi_{\phi r}} - C_{L_t}\frac{|a_t|}{|r|}e^{i\Phi_{a_t r}} = 0$$

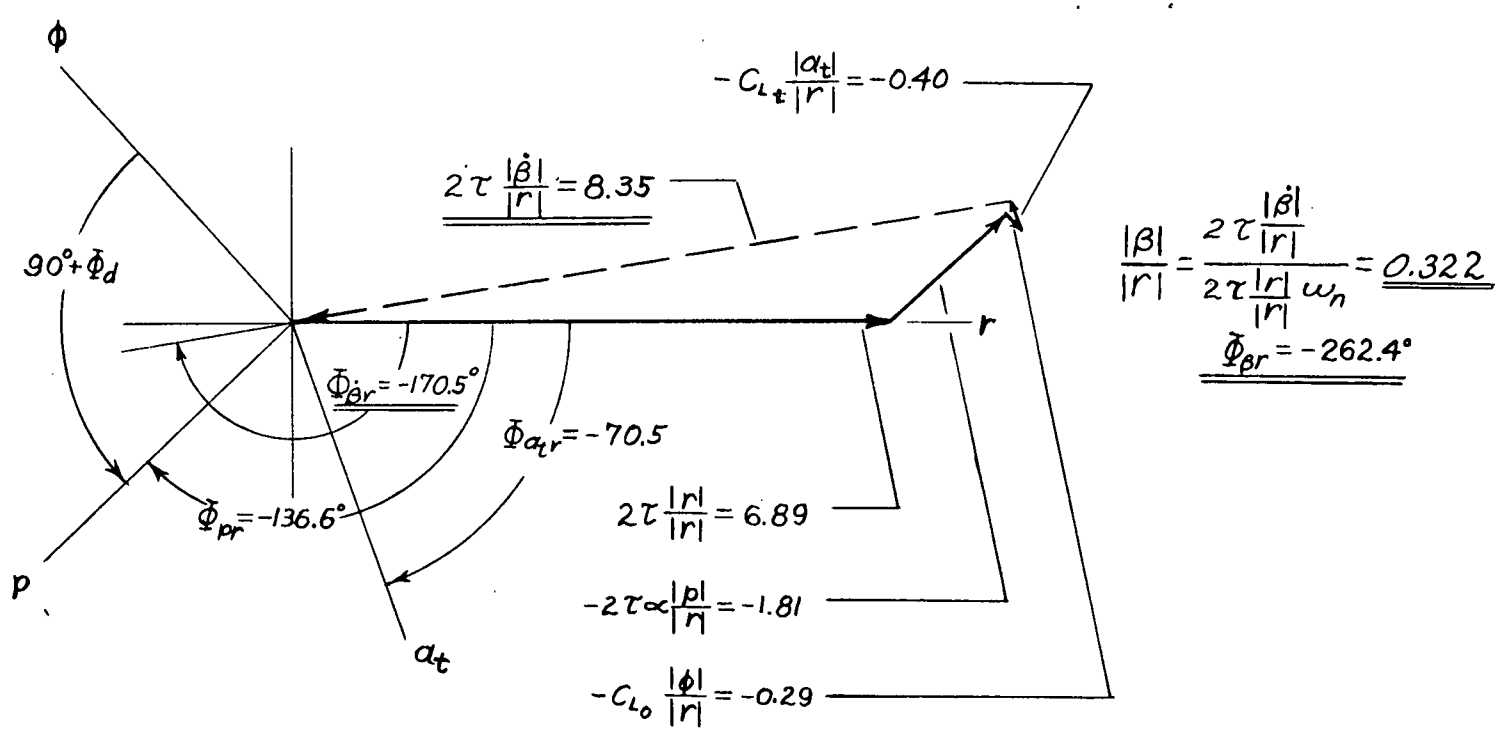

(a) Determination of $\frac{|\beta|}{|r|}$ and $\Phi_{\beta r}$.

Figure 26.- A typical time-vector solution of rolling- and yawing-stability derivatives.

$$\frac{I_z}{\bar{q}Sb}\frac{|\dot{r}|}{|r|}e^{i\Phi_{\dot{r}r}} - \frac{I_{xz}}{\bar{q}Sb}\frac{|\dot{p}|}{|r|}e^{i\Phi_{\dot{p}r}} - C_{n_\beta}\frac{|\beta|}{|r|}e^{i\Phi_{\beta r}} - C_{n_p}\frac{|p'|}{|r|}e^{i\Phi_{pr}} - (C_{n_r} - C_{n_{\dot{\beta}}})\frac{|r'|}{|r|}e^{i\Phi_{rr}} = 0$$

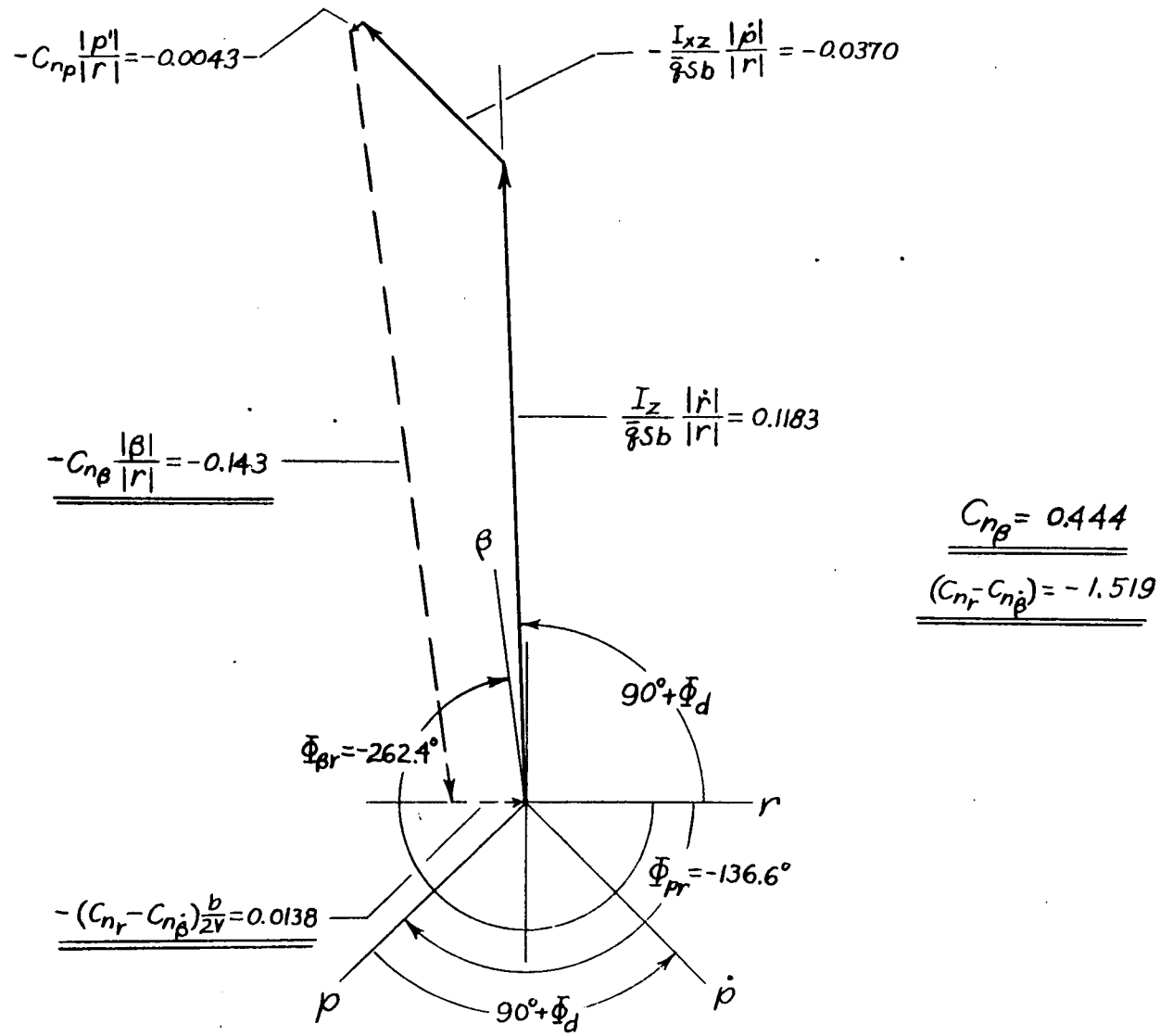

(b) Determination of C_{n_β} and $(C_{n_r} - C_{n_{\dot{\beta}}})$.

Figure 26.- Continued.

$$\frac{I_x}{\bar{q}Sb}\frac{|\dot{p}|}{|r|}e^{i\Phi_{\dot{p}r}} - \frac{I_{xz}}{\bar{q}Sb}\frac{|\dot{r}|}{|r|}e^{i\Phi_{\dot{r}r}} - C_{l_\beta}\frac{|\beta|}{|r|}e^{i\Phi_{\beta r}} - C_{l_p}\frac{|p'|}{|r|}e^{i\Phi_{pr}} - C_{l_r}\frac{|r'|}{|r|}e^{i\Phi_{rr}} = 0$$

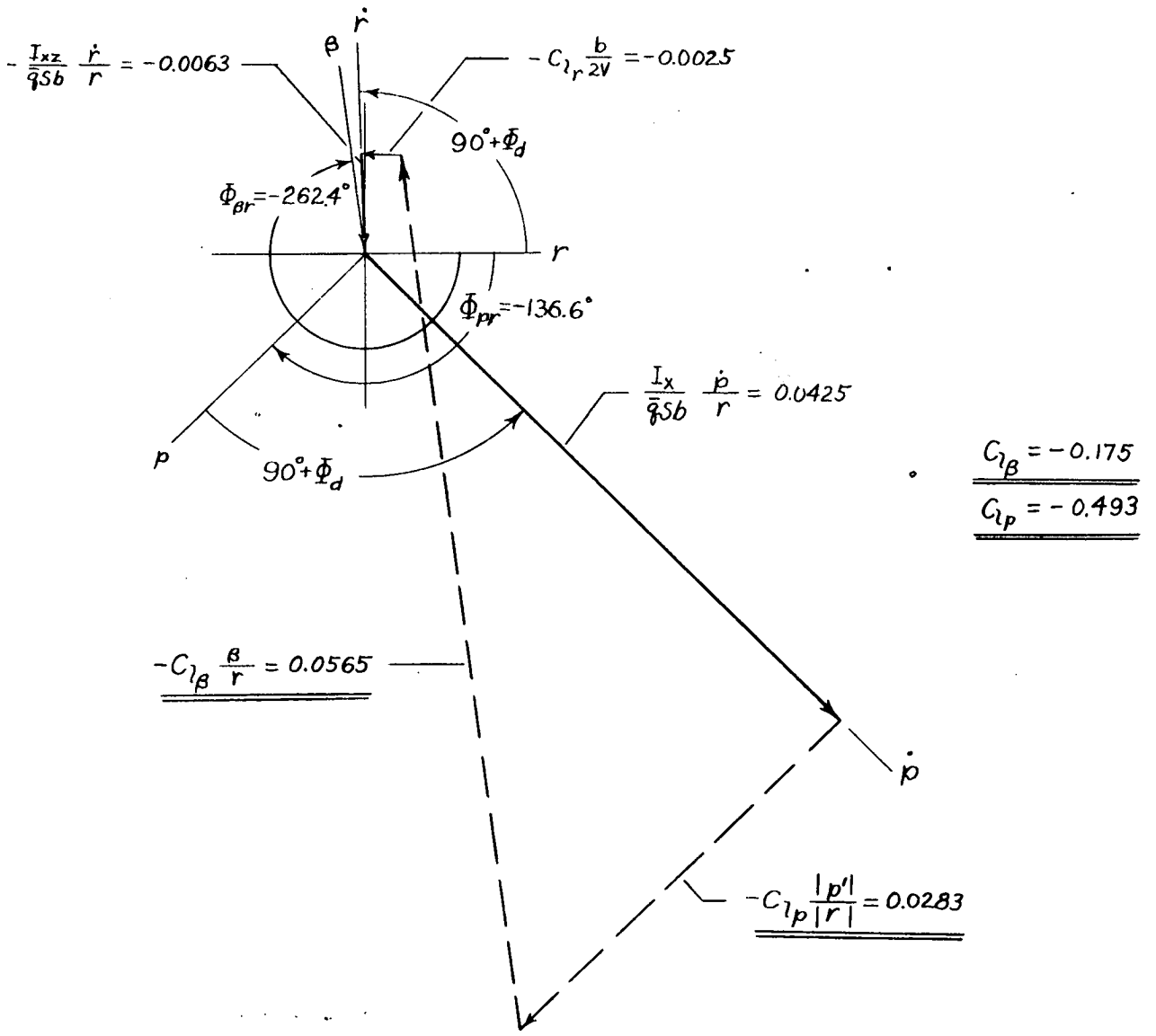

(c) Determination of C_{l_β} and C_{l_p}.

Figure 26.- Concluded.